The production and escape of Lyman-Continuum radiation from star-forming galaxies at z ∼ 2 and their redshift evolution

Jorryt Matthee[1]⋆, David Sobral[1,2], Philip Best[3], Ali Ahmad Khostovan[4], Ivan Oteo[3,5], Rychard Bouwens[1], Huub Röttgering[1]

[1] *Leiden Observatory, Leiden University, P.O. Box 9513, NL-2300 RA Leiden, The Netherlands*
[2] *Department of Physics, Lancaster University, Lancaster, LA1 4YB, UK*
[3] *Institute for Astronomy, University of Edinburgh, Royal Observatory, Blackford Hill, Edinburgh EH9 3HJ UK*
[4] *University of California, Riverside, 900 University Ave, Riverside, CA, 92521, USA*
[5] *European Southern Observatory, Karl-Schwarzschild-Str. 2, 85748 Garching, Germany*

31 May 2016

ABSTRACT

We study the production and escape of ionizing photons of a sample of 588 Hα emitters (HAEs) at $z = 2.2$ in COSMOS by exploring their rest-frame Lyman Continuum (LyC) with *GALEX/NUV* data. We find 8 candidate LyC leakers with $\mathrm{f_{esc}} > 60$ % out of a clean subsample of 191 HAEs (i.e. without any neighbour or foreground galaxy inside the *GALEX* PSF). Overall, we measure a very low escape fraction $\mathrm{f_{esc}} < 5.5\,(12.7)$% through median (mean) stacking. By combining the Hα luminosity density with IGM emissivity measurements from absorption studies, we find a globally averaged $\langle \mathrm{f_{esc}} \rangle$ of $5.9^{+9.3}_{-2.6}$ %. We find similarly low values of the global $\langle \mathrm{f_{esc}} \rangle$ at $z \approx 3-5$, indicating little evolution of $\langle \mathrm{f_{esc}} \rangle$ with redshift and ruling out a high $\langle \mathrm{f_{esc}} \rangle$ at $z < 5$. We also measure the typical number of ionizing photons per unit UV luminosity, $\xi_{ion} \approx 10^{24.77\pm0.04}$ Hz erg^{-1}. HAEs at $z = 2.2$ are typically three times less ionizing than typically assumed in the reionization era, but higher values of ξ_{ion} are found for galaxies with strong Lyman-α and lower mass. Due to an increasing ξ_{ion} with increasing EW(Hα), ξ_{ion} likely increases with redshift. This evolution alone is fully in line with the observed evolution of ξ_{ion} between $z \approx 2-5$, indicating a typical value of $\xi_{ion} \approx 10^{25.4}$ Hz erg^{-1} in the reionization era. Therefore, only modest global escape fractions of ~ 10 % are required to provide enough photons to reionize the Universe. Our results are consistent with only a few galaxies having $\mathrm{f_{esc}} \approx 75$ %, which could indicate that a small fraction $(4 \pm 1$ %) of galaxies contribute most of the total number of escaping ionizing photons.

Key words: galaxies: high-redshift – galaxies: evolution – cosmology:observations – cosmology: dark ages, re-ionisation, first stars.

1 INTRODUCTION

One of the most important questions in galaxy formation is whether galaxies alone have been able to provide the ionizing photons which reionized the Universe. Optical depth measurements from the Planck satellite place the mean reionization redshift between $z \approx 7.8 - 8.8$ (Planck Collaboration et al. 2016). The end-point of reionization has been marked by the Gun-Peterson trough in high-redshift quasars at $z \approx 5 - 6$, with a typical neutral fraction of $\sim 10^{-4}$ (e.g.

Fan et al. 2006; McGreer et al. 2015). Moreover, recent observations indicate that there are large opacity fluctuations among various sight-lines, indicating an inhomogeneous nature of reionization (Becker et al. 2015).

　　Assessing whether galaxies have been the main provider of ionizing photons at $z \gtrsim 5$ (alternatively to Active Galactic Nucleii, AGN; e.g. Madau & Haardt 2015; Giallongo et al. 2015; Weigel et al. 2015) crucially depends on i) precise measurements of the number of galaxies at early cosmic times, ii) the clumping factor of the IGM (e.g. Pawlik et al. 2015), iii) the amount of ionizing photons that is produced (Lyman-Continuum photons, LyC, $\lambda < 912$Å) and iv) the fraction of

⋆ E-mail: matthee@strw.leidenuniv.nl

ionizing photons that escapes into the inter galactic medium (IGM). All these numbers are currently uncertain, with the relative uncertainty greatly rising from i) to iv).

Many studies so far have focussed on counting the number of galaxies as a function of their UV luminosity (luminosity functions) at $z > 7$ (e.g. McLure et al. 2013; Bowler et al. 2014; Atek et al. 2015; Bouwens et al. 2015a; Finkelstein et al. 2015; Ishigaki et al. 2015; McLeod et al. 2015; Castellano et al. 2016; Livermore et al. 2016). These studies typically infer luminosity functions with steep faint-end slopes ($\alpha \approx -2$, see also Reddy & Steidel 2009 at $z \sim 2-3$), and a steepening of the faint-end slope with increasing redshift (see for example the recent review from Finkelstein 2015), leading to a high number of faint galaxies. Assuming "standard" values for the other parameters such as the escape fraction, simplistic models indicate that galaxies may indeed have provided the ionizing photons to reionize the Universe (e.g. Madau et al. 1999; Robertson et al. 2015), and that the ionizing background at $z \sim 5$ is consistent with the derived emissivity from galaxies (Choudhury et al. 2015; Bouwens et al. 2015b). However, without validation of input assumptions regarding the production and escape of ionizing photons (for example, these simplistic models assume that the escape fraction does not depend on UV luminosity), the usability of these models remains to be evaluated.

The amount of ionizing photons that are produced per unit UV (rest-frame ≈ 1500 Å) luminosity (ξ_{ion}) is generally calculated using SED modelling (e.g. Madau et al. 1999; Bouwens et al. 2012; Kuhlen & Faucher-Giguère 2012) or (in a related method) estimated from the observed values of the UV slopes of high-redshift galaxies (e.g. Robertson et al. 2013; Duncan & Conselice 2015). Most of these studies find values around $\xi_{ion} \approx 10^{25.2-25.3}$ Hz erg^{-1} at $z \sim 8$. More recently, Bouwens et al. (2016) estimated the number of ionizing photons in a sample of Lyman break galaxies (LBGs) at $z \sim 4$ to be $\xi_{ion} \approx 10^{25.3}$ Hz erg^{-1} by estimating Hα luminosities with *Spitzer*/IRAC photometry.

The most commonly adopted escape fraction of ionizing photons, f_{esc}, is 10-20 %, independent of mass or luminosity (e.g. Mitra et al. 2015; Robertson et al. 2015). However, hydrodynamical simulations indicate that f_{esc} is likely very anisotropic and time dependent (Cen & Kimm 2015; Ma et al. 2015). An escape fraction which depends on galaxy properties (for example a higher f_{esc} for lower mass galaxies, e.g. Paardekooper et al. 2015) would influence the way reionization happened (e.g. Sharma et al. 2016). Most importantly, it is impossible to measure f_{esc} directly at high-redshift ($z > 6$) because of the high opacity of the IGM for ionizing photons (e.g. Inoue et al. 2014). Furthermore, to estimate f_{esc} it is required that the intrinsic amount of ionizing photons is measured accurately, which requires accurate understanding of the stellar populations, SFR and dust attenuation (c.f. De Barros et al. 2016).

Nevertheless, several attempts have been made to measure f_{esc}, both in the local Universe (e.g. Leitherer et al. 1995; Deharveng et al. 2001; Leitet et al. 2013; Alexandroff et al. 2015) and at intermediate redshift, $z \sim 3$, where it is possible to observe redshifted LyC radiation with optical CCDs (e.g. Inoue et al. 2006; Boutsia et al. 2011; Vanzella et al. 2012; Bergvall et al. 2013; Mostardi et al. 2015). However, the number of reliable direct detections is limited to a handful, both in the local Universe and at intermediate red-

shift (e.g. Borthakur et al. 2014; Izotov et al. 2016b,a; De Barros et al. 2016; Leitherer et al. 2016), and strong limits of $f_{esc} \lesssim 5-10$ % exist for the majority (e.g. Grazian et al. 2016; Guaita et al. 2016). An important reason is that contamination from sources in the foreground may mimic escaping LyC, and high resolution UV imaging is thus required (e.g. Mostardi et al. 2015; Siana et al. 2015). Even for sources with established LyC leakage, estimating f_{esc} reliably depends on the ability to accurately estimate the intrinsically produced amount of LyC photons and precisely model the transmission of the IGM (e.g. Vanzella et al. 2016).

Progress can be made by expanding the searched parameter space to lower redshifts, where rest-frame optical emission lines (e.g. Hα) can provide valuable information on the production rate of LyC photons. In addition, galaxy samples obtained from large volumes are required to unveil rare objects with high escape fractions (which could dominate global emissivity from galaxies if their escape fraction is high enough). Recently, Rutkowski et al. (2016) combined a large sample of relatively faint star-forming galaxies (SFGs) at $z \sim 1$ to obtain strong median upper limits ($f_{esc} \lesssim 3$ %, see also Cowie et al. 2009; Bridge et al. 2010) by stacking relatively shallow *GALEX* UV data. Sandberg et al. (2015) combined ten $z = 2.2$ Hα emitters with deep *HST* UV data, but obtained less strict upper limits ($f_{esc} \lesssim 24$ %) due to a relatively small sample size and low SFRs. Neither Rutkowski et al. (2016) nor Sandberg et al. (2015) find any candidate LyC leaker.

In this paper, we use a large sample of Hα emitters (HAEs) at $z = 2.2$ to measure the production and escape of ionizing photons and how these may depend on galaxy properties. We constrain f_{esc} using archival *GALEX NUV* imaging. Our sample size and UV data are similar to that of Rutkowski et al. (2016), but our typical galaxy has an order of magnitude higher star formation rate (SFR). This is because our galaxies are selected from wide-field surveys and the typical SFR of galaxies at $z \sim 2$ is higher than at $z \sim 1$ (see e.g. Madau & Dickinson 2014 and references therein). While our UV imaging is shallower than the data used by Sandberg et al. (2015) at the same redshift, we have ~ 80 times more sources, with a typically higher SFR. Similar to these surveys, we can accurately measure the intrinsic production of ionizing photons with Hα measurements and compare the estimated emissivity of HAEs with IGM emissivity measurements from quasar absorption lines (e.g. Becker & Bolton 2013). Combined with rest-frame UV photometry, accurate measurements of ξ_{ion} are allowed on a source by source basis, allowing us to explore correlations with galaxy properties. We also measure the median ξ_{ion} from stacks of Lyman-α emitters from Sobral et al. (2016a).

We describe the galaxy sample and definitions of galaxy properties in §2. §3 presents the *GALEX* imaging. We present measurements of f_{esc} in §4. We indirectly estimate f_{esc} from the Hα luminosity function and the IGM emissivity in §5 and measure the ionizing properties of galaxies and its redshift evolution in §6. §7 discusses the implications for reionization. Finally, our results are summarised in §8. We adopt a ΛCDM cosmology with $H_0 = 70$ km s^{-1}Mpc^{-1}, $\Omega_M = 0.3$ and $\Omega_\Lambda = 0.7$. Magnitudes are in the AB system. At $z = 2.2$, $1''$ corresponds to a physical scale of 8.2 kpc.
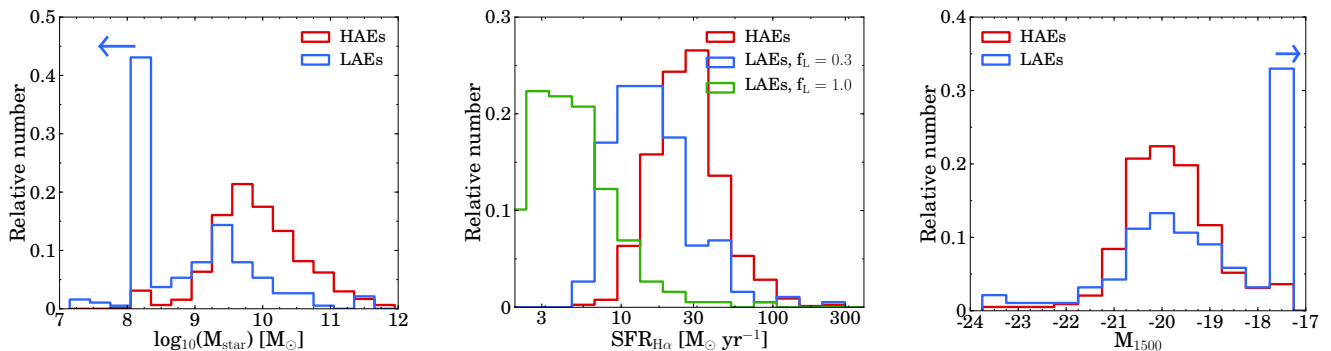
Figure 1. Histogram of the properties of HAEs and LAEs. Stellar mass is obtained through SED fitting (see §2.1.1). For HAEs, SFR(Hα) is obtained from dust-corrected Hα. LAEs which are undetected in broad-bands (and thus without SED fits) are assigned $M_{star} = 10^8$ $M_\odot$ and $M_{1500} = -17$, corresponding to a V band limit of 27 and we assumed those galaxies have no dust in computing SFR(Hα). For LAEs, we use the observed Lyα luminosity and convert this to Hα for two different Lyα escape fractions (f$_L$, the typical escape fraction for LAEs (30 %) and the maximum of 100 %, see Sobral et al. 2016a). M_{1500} is obtained by converting the observed V magnitude to absolute magnitude. In general, LAEs trace a galaxy population with lower stellar masses and SFR and fainter UV magnitudes.

2 GALAXY SAMPLE

We use a sample of Hα selected star-forming galaxies from the High-z Emission Line Survey (HiZELS; Geach et al. 2008; Sobral et al. 2009; Best et al. 2013; Sobral et al. 2013) at $z = 2.2$ in the COSMOS field. These galaxies were selected using narrow-band (NB) imaging in the K band with the United Kingdom InfraRed Telescope. Hα emitters (HAEs) were identified among the line-emitters using BzK and BRU colours and photometric redshifts, as described in Sobral et al. (2013). In total, there are 588 Hα emitters at $z = 2.2$ in COSMOS.[1]

HAEs are selected to have EW$_{0,H\alpha+[NII]}$ > 25 Å. Since the COSMOS field has been covered by multiple narrow-band filters, a fraction of $z = 2.2$ sources are detected with multiple major emission lines in addition to Hα: [OIII], [OII] (e.g. Sobral et al. 2012; Nakajima et al. 2012; Sobral et al. 2013) or Lyα (e.g. Oteo et al. 2015; Matthee et al. 2016). Multi-wavelength photometry from the observed UV to mid-IR is widely available in COSMOS. In this paper, we make explicit use of V and R band in order to measure the UV luminosity and UV slope β (see §2.1.3), but all bands have been used for photometric redshifts (see Sobral et al. 2013, and e.g. Ilbert et al. 2009) and SED fitting (Sobral et al. 2014; Oteo et al. 2015; Khostovan et al. 2016).

We also include 160 Lyman-α emitters (LAEs) at $z = 2.2$ from the CAlibrating LYMan-α with Hα survey (CA-LYMHA; Matthee et al. 2016; Sobral et al. 2016a). For completeness at bright luminosities, LAEs were selected with EW$_{0,Ly\alpha}$ > 5 Å, while LAEs are typically selected with a higher EW cut of 25 Å (see e.g. Matthee et al. 2015 and references therein). However, only 15 % of our LAEs have EW$_{0,Ly\alpha}$ < 25 Å and these are typically AGN, see Sobral et al. (2016a). We note that 40 % of LAEs are too faint to be detected in broad-bands, and we thus have only upper limits on it stellar mass and UV magnitude (see Fig. 1). By design, CALYMHA observes both Lyα and Hα for Hα selected galaxies. As presented in Matthee et al. (2016),

17 HAEs are also detected in Lyα with the current depth. These are considered as HAEs in the remainder of the paper.

We show the general properties of our sample of galaxies in Fig. 1. It can be seen that compared to HAEs, LAEs are typically somewhat fainter in the UV, have a lower mass and lower SFR, although they are also some of the brightest UV objects.

Our sample of HAEs and LAEs was chosen for the following reasons: i) all are at the same redshift slice where the LyC can be efficiently observed with the *GALEX NUV* filter and Hα with the NB$_K$ filter, ii) the sample spans a large range in mass, star formation rate (SFR) and environments (Fig. 1 and Sobral et al. 2014) and iii) as discussed in Oteo et al. (2015), Hα selected galaxies span the entire range of star-forming galaxies, from dust-free to relatively dust-rich (unlike e.g. Lyman-break galaxies).

2.1 Definition of galaxy properties

We define the galaxy properties that are used in the analysis in this subsection. These properties are either obtained from: (1) SED fitting of the multi-wavelength photometry, (2) observed Hα flux, or (3) observed rest-frame UV photometry.

2.1.1 SED fitting

For HAEs, stellar masses (M_{star}) and stellar dust attenuations (E($B-V$)) are taken from Sobral et al. (2014). In this study, synthetic galaxy SEDs are simulated with Bruzual & Charlot (2003) stellar templates with metallicities ranging from $Z = 0.0001 - 0.05$, following a Chabrier (2003) initial mass function (IMF) and with exponentially declining star formation histories. The dust attenuation is described by a Calzetti et al. (2000) law. The observed UV to IR photometry is then fitted to these synthetic SEDs. The values of M_{star} and E($B-V$) that we use are the median values of all synthetic models which have a χ^2 within 1σ of the best fitted model. The 1σ uncertainties are typically $0.1 - 0.2$ dex for M_{star} and 0.05-0.1 dex for E($B-V$). The smallest errors are found at high masses and high extinctions. The same SED

---

[1] The sample of Hα emitters from Sobral et al. (2013) is publicly available through e.g. VizieR, http://vizier.cfa.harvard.edu.

fitting method is applied to the photometry of LAEs. Our sample spans galaxies with masses $M_{star} = 10^{7.5-12}$ $M_\odot$, see Fig. 1.

2.1.2 Intrinsic Hα luminosity

The intrinsic Hα luminosity is used to compute instantaneous star formation rates (SFRs) and the number of produced ionizing photons. To measure the intrinsic Hα luminosity, we first correct the observed line-flux in the NB_K filter for the contribution of the adjacent [NII] emission-line doublet. We also correct the observed line-flux for attenuation due to dust.

We correct for the contribution from [NII] using the relation between [NII]/Hα and $EW_{0,[NII]+Hα}$ from Sobral et al. (2012). This relation holds up to at least $z \sim 1$ (Sobral et al. 2015a) and the median ratio of [NII]/(Hα+ [NII]) = 0.2 is consistent with spectroscopic follow-up at $z \approx 2$ (e.g. Swinbank et al. 2012; Sanders et al. 2015).

Attenuation due to dust is estimated with a Calzetti et al. (2000) attenuation curve and by assuming that the nebular attenuation equals the stellar attenuation, $E(B - V)_{gas} = E(B - V)_{stars}$. This is in agreement with the average results from the Hα sample from MOSDEF (Shivaei et al. 2015), although we note that there are indications that the nebular attenuation is stronger for galaxies with higher SFRs and masses (e.g. Reddy et al. 2015; Puglisi et al. 2016) and other studies indicate slightly higher nebular attenuations (e.g. Förster Schreiber et al. 2009; Wuyts et al. 2011; Kashino et al. 2013). We note that we vary the method to correct for dust in the relevant sections (e.g. §6.3) in two ways: either based on the UV slope (Meurer et al. 1999), or from the local relation between dust attenuation and stellar mass (Garn & Best 2010)).

Star formation rates are obtained from dust-corrected L(Hα) and using a Chabrier (2003) initial mass function: SFR = 4.4×10^{-42} L(Hα) (e.g. Kennicutt 1998), where the SFR is in $M_\odot$ yr^{-1} and L(Hα) in erg s^{-1}. The SFRs of galaxies in our sample range from $3 - 300$ $M_\odot$ yr^{-1}, with a typical SFR of ≈ 30 $M_\odot$ yr^{-1}, see Fig. 1.

2.1.3 Rest-frame UV photometry and UV slopes

For our galaxy sample at $z = 2.2$, the rest-frame UV ($\sim$ 1500Å) is traced by the V band, which is not contaminated by (possibly) strong Lyα emission.

We correct the UV luminosities from the V band for dust with the Calzetti et al. (2000) attenuation curve and the fitted $E(B - V)$ values. The absolute magnitude, M_{1500}, is obtained by subtracting a distance modulus of $\mu = 44.97$ (obtained from the luminosity distance and corrected for bandwidth stretching with $2.5\log_{10}(1+z)$, $z = 2.23$) from the observed V band magnitudes. The UV slope β is measured with observed V and R magnitudes following:

$$\beta = -\frac{V - R}{2.5\log_{10}(\lambda_V/\lambda_R)} - 2 \qquad (1)$$

Here, $\lambda_V = 5477.83$ Å, the effective wavelength of the V filter and $\lambda_R = 6288.71$ Å, the effective wavelength of the R filter. With this combination of filters, β is measured around a rest-frame wavelength of ~ 1800 Å.
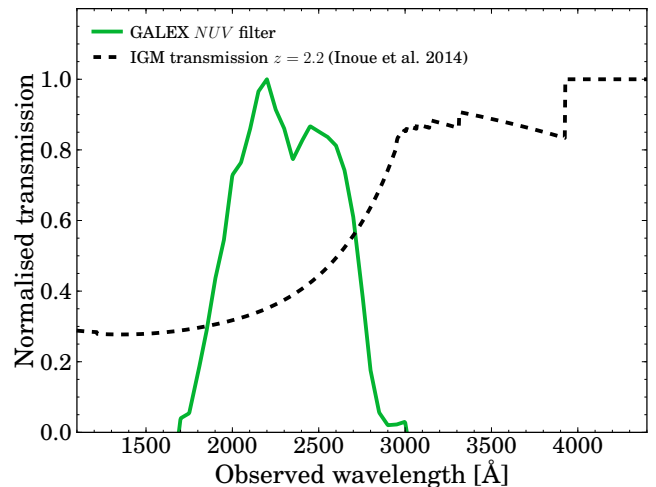

Figure 2. Filter transmission of the *GALEX NUV* filter (green line) and mean IGM transmission versus observed wavelength (dashed black line). We compute the IGM transmission at $z = 2.2$ using the models from Inoue et al. (2014). The bandpass-averaged IGM transmission is 40.4 %. As highlighted by a simulation from Vasei et al. 2016, the mean value of T_{IGM} is not the most common value. The distribution is bimodal, with a narrow peak at $T_{IGM} \approx 0.0$ and a broad peak around $T_{IGM} = 0.7$.

3   *GALEX* UV DATA

For galaxies observed at $z = 2.2$, rest-frame LyC photons can be observed with the NUV filter on the *GALEX* space telescope. In COSMOS there is deep *GALEX* data (3σ AB magnitude limit ~ 25, see e.g. Martin et al. 2005; Muzzin et al. 2013) available from the public Deep Imaging Survey. We stress that the full width half maximum (FWHM) of the point spread function (PSF) of the NUV imaging is 5.4″(Martin et al. 2003) and that the pixel scale is 1.5″ pix^{-1}. We have acquired NUV images in COSMOS from the Mikulski Archive at the Space Telescope Science Institute (MAST)[2]. All HAEs and LAEs in COSMOS are covered by *GALEX* observations, due to the large circular field of view with 1.25 degree diameter. Five pointings in the COSMOS field overlap in the center, which results in a total median exposure time of 91.4 ks and a maximum exposure time of 236.8 ks.

3.1   Removing foreground/neighbouring contamination

The large PSF-FWHM of *GALEX NUV* imaging leads to a major limitation in measuring escaping LyC photons from galaxies at $z = 2.2$. This is because the observed flux in the NUV filter could (partly) be coming from a neighbouring foreground source at lower redshift. In order to overcome this limitation, we use available high resolution deep optical *HST*/ACS F814W (rest-frame ≈ 2500 Å, Koekemoer et al. 2007) imaging to identify sources for which the NUV flux

---

[2] https://mast.stsci.edu/

might be confused due to possible foreground or neighbouring sources and remove these sources from the sample. In addition, we use visual inspections of deep ground-based U band imaging as a cross-check for the bluest sources which may be missed with the *HST* imaging. These data are available through the COSMOS archive.[3]

Neighbours are identified using the photometric catalog from Ilbert et al. (2009), which is selected on deep *HST*/ACS F814W data. We find that 195 out of the 588 HAEs in COSMOS have no neighbour inside a radius of 2.7″. We refer to this subsample as our CLEAN sample of galaxies in the remainder of the text. The average properties (dust attenuation, UV magnitude mass and SFR) of this sample is similar to the full sample of SFGs.

4   THE ESCAPE FRACTION OF IONIZING PHOTONS

4.1   How to measure f_{esc}?

The escape fraction of ionizing photons, f_{esc} can be measured directly from the ratio of observed to intrinsic LyC luminosity. Rest-frame LyC photons are redshifted into the *NUV* filter at $z = 2.2$. However, the IGM between $z = 2.2$ and our telescopes is not transparent to LyC photons (see Fig. 2), such that we need to correct the observed LyC luminosity for IGM absorption.

The intrinsic number of emitted ionizing photons per second, Q_{ion}) can be estimated from the strength of the (dust corrected) Hα emission line as follows:

$$L_{H\alpha} = Q_{ion} \, c_{H\alpha} \, (1 - f_{esc}) \tag{2}$$

where Q_{ion} is in s^{-1}, $L_{H\alpha}$ is in erg s^{-1} and f_{esc} is the escape fraction of ionizing photons, while $c_{H\alpha} = 1.36 \times 10^{-12}$ erg (e.g. Kennicutt 1998; Schaerer 2003) for case B recombinations with a temperature of $T = 10\,000$ K. The observed luminosity in the *NUV* filter (L_{NUV}) is related to the number of ionizing photons as:

$$L_{NUV} = Q_{ion} \, \epsilon \, f_{esc} \, T_{IGM,NUV} \tag{3}$$

Here, ϵ is the average energy of an ionizing photon observed in the *NUV* filter (which traces rest-frame wavelengths from 550 to 880 Å, see Fig. 2). By exploring STARBURST99 (Leitherer et al. 1999) SED models, we investigate how ϵ depends on the properties of stellar populations. We assume a single burst of star formation with a Salpeter IMF with upper mass limit 100 M$_\odot$, Geneva stellar templates without rotation (Mowlavi et al. 2012) and metallicity $Z = 0.02$. We find that ϵ is a strong function of age, but that it is strongly correlated with the EW of the Hα line (which itself also is a strong function of age). For the range of Hα EWs in our sample, $\epsilon = 17.04^{+0.45}_{-0.26}$ eV. We therefore take $\epsilon = 17.0$ eV.

$T_{IGM,NUV}$ is the absorption of LyC photons due to the intervening IGM, convolved with the *NUV* filter. Note that $T_{IGM} = e^{-\tau_{IGM}}$, where τ_{IGM} is the optical depth to LyC photons in the IGM, see e.g Vanzella et al. (2012). The IGM transmission depends on the wavelength and redshift. According to the model of Inoue et al. (2014), the mean IGM

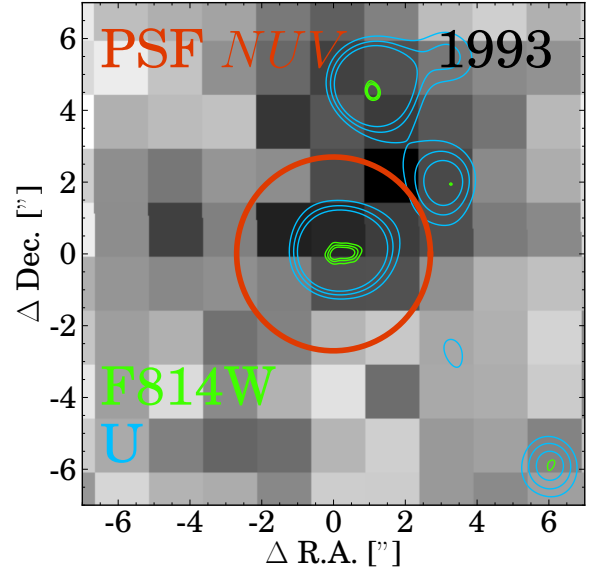[3] http://irsa.ipac.caltech.edu/data/COSMOS/

Figure 3. $15 \times 15''$ thumbnail image of the isolated LyC leaker candidate with HiZELS ID 1993. The background image shows the counts in *GALEX NUV* imaging. The green contours correspond to the 3, 4 and 5 σ contours in the HST/ACS F814W image, smoothed with the PSF FWHM of 0.09″ (Scoville et al. 2007), while the blue contours are from CFHT/U band imaging (McCracken et al. 2010). The red circle shows the PSF of the *NUV* image. Source 1993 is detected in Lyα, Hα and [OIII]. Part of the *NUV* flux may be contributed by a nearby source as indicated from the U band contours. We note that the two companion sources have photometric redshifts 0.6 and 1.1 respectively.

transmission for LyC radiation at $\lambda \sim 750$ Å for a source at $z = 2.2$ is $T_{IGM} \approx 40$ %. We convolve the IGM transmission as a function of observed wavelength for a source at $z = 2.2$ with the normalised transmission of the *NUV* filter, see Fig. 2. This results in a bandpass-averaged $T_{IGM,NUV} = 40.4\%$.

Combining equations 2 and 3 results in:

$$f_{esc} = (1 + \alpha \frac{L_{H\alpha}}{L_{NUV}})^{-1} \tag{4}$$

where we define $\alpha = \epsilon \, c_{H\alpha}^{-1} \, T_{IGM,NUV}$. Combining our assumed values, we estimate $\alpha = 8.09$. Note that we investigate the systematic uncertainties of this value in §4.4.2.

In addition to the absolute escape fraction of ionizing radiation, it is common to define the relative escape fraction of LyC photons to UV (~ 1500 Å) photons, since these are most commonly observed in high redshift galaxies. Following Steidel et al. (2001), the relative escape fraction, f_{esc}^{rel}, is defined as:

$$f_{esc}^{rel} = f_{esc} e^{\tau_{dust,UV}} = \frac{(L_{UV}/L_{NUV})_{int}}{(L_{UV}/L_{NUV})_{obs}} T_{IGM,NUV}^{-1} \tag{5}$$

In this equation, L_{UV} is the luminosity in the observed V band, $e^{\tau_{dust,UV}}$ is the correction for dust (see §2.1.3) and we adopt an intrinsic ratio of $(L_{UV}/L_{NUV})_{int} = 5$ (e.g. Siana et al. 2007). The relative escape fraction can be related to the absolute escape fraction when the dust attenuation for L_{UV}, A_{UV}, is known: $f_{esc} = f_{esc}^{rel} \times 10^{-0.4 A_{UV}}$.

Table 1. Candidate LyC leakers among the Hα sample. ID numbers refer to the IDs in the HiZELS catalog (Sobral et al. 2013). IDs indicated with a * are X-Ray AGN. Note that f_{esc} is an upper limit because minor blending of nearby sources increases the observed NUV flux, see for example Fig. 3.

ID	M_{star} $\log_{10}(M_{\odot})$	$SFR(H\alpha)$ $M_{\odot} \ yr^{-1}$	M_{1500} mag	NUV mag	f_{esc} %
1139*	10.22	34.8	-21.6	25.9	60
1872	9.45	9.2	-21.0	25.7	87
1993	9.85	8.2	-21.3	24.6	94
2258	10.50	7.3	-21.0	25.1	89
4349	10.63	13.4	-19.8	25.8	70
7801*	10.52	43.3	-23.5	24.9	75
8760	9.34	18.1	-20.6	24.5	90
8954	9.16	18.2	-19.5	25.8	62

4.2 Individual detections

We search for individual galaxies leaking LyC photons by matching our CLEAN galaxy sample with the public *GALEX* EM cleaned catalogue (e.g. Zamojski et al. 2007; Conseil et al. 2011), which is U band detected. In total, we find 19 matches between CLEAN HAEs and *GALEX* sources with $NUV < 26$ within $1''$ (33 matches when using all HAEs), and 9 matches between LAEs and *GALEX* sources (four out of these 9 are also in the HAE sample and we will discuss these as HAEs). By visual inspection of the *HST*/ACS F814W and CFHT/U band imaging, we mark 8/19 HAEs and 2/5 LAEs as reliable candidate LyC leakers. The 14 matches that we discarded were either unreliable detections in NUV (9 times, caused by local variations in the depth, such that the detections are at 2σ level) or a fake source in NUV (5 times, caused by artefacts of bright objects). We note however that in most of our 10 candidate LyC leakers (8 HAEs, 2 LAEs) the NUV photometry is slightly blended with a source at a distance of $\approx 4''$, see Fig. A1.

In order to estimate the LyC escape fraction for the 8 HAE candidate LyC leakers, we use NUV photometry from the EMPHOT COSMOS catalogue. Assuming that all the NUV flux originates from the source at $z = 2.2$, we measure escape fractions ranging from $\approx 60 - 90$ %, see Table 1. As most of our sources seem to be slightly blended with nearby sources, these escape fractions are upper limits. Observations with higher spatial resolution are required in order to confirm whether these 10 candidates are really leaking LyC photons and at what rate.

Four isolated LyC leaker candidates (including two LAEs) are X-Ray AGN, and all have been spectroscopically confirmed at $z = 2.2$ (Lilly et al. 2009; Civano et al. 2012). Contrarily to the typical assumption that $f_{esc} = 100$ % in AGN (e.g. Madau & Haardt 2015), we find that these AGN have lower escape fractions of ≈ 70 %, more consistent with recent measurements (Cristiani et al. 2016; Micheva et al. 2016), and with important implications for the contribution of AGN to the ionizing background (discussed further in §5.1).

We show the thumbnail NUV image of one of the best star-forming candidate LyC leakers in Fig. 3, where we also indicate the contours of the rest-frame UV as observed in the U band from CFHT and the F814W band from *HST*. This source (HiZELS-ID 1993) is detected in Lyα ($EW_{0,Ly\alpha} = 67$
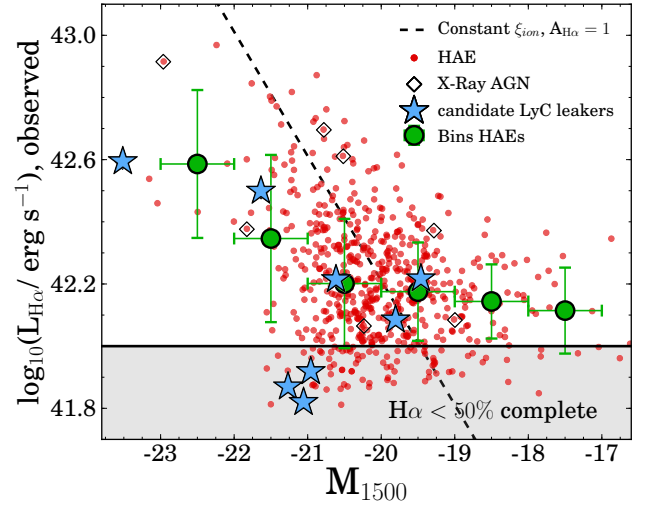

Figure 4. M_{1500} versus $L_{H\alpha}$, without correcting for dust (red points), for HAEs at $z = 2.2$. We indicate the luminosities where our Hα selection is less than 50 % complete (see Sobral et al. 2013). The green points show the median and standard deviation (as error) for bins in $L_{H\alpha}$. The black dashed line shows the expected Hα luminosity for a constant $\xi_{ion} = 10^{24.6}$ Hz erg^{-1} and $A_{H\alpha} = 1.0$. This line shifts right with increasing dust attenuation or ξ_{ion} and flattens somewhat if the dust attenuation is lower for UV bright galaxies. Below a UV magnitude of $M_{1500} \approx -20.5$, our selection preferably picks up sources with high Hα to UV ratio. It can be seen that AGN typically have a high Hα to UV ratio, and that some candidate LyC leakers (blue stars) lie below the mean relation, which is consistent with not all their ionizing photons having recombined into Hα luminosity.

Å) and [OIII], with $EW_{0,[OIII]} > 100$ Å and a (maximum) escape fraction of ≈ 90 %. Thumbnails of all LyC candidates are shown in the appendix (Fig. A1).

The candidate LyC leakers are on average bluer and less dusty than the average HAE. As illustrated in Fig. 4, four LyC leakers lie significantly below the average relation between observed Hα luminosity and UV magnitude. This is expected to be the case for a high f_{esc}, since that will decrease the observed Hα luminosity (see Eq. 2). If f_{esc} for these sources would have been 0 % (instead of $\approx 60 - 70$ %, see Table 1), the Hα luminosity would have been ≈ 0.5 dex higher, which would place them on the median relation between Hα luminosity and UV magnitude. This seems to support the reality of these candidate LyC leakers.

This preliminary sample of LyC leakers allows us to investigate predictions from Zackrisson et al. (2013), who argue that galaxies with high f_{esc} can be identified using their UV slopes and Hβ EWs. We find that at fixed UV slopes, seven of our candidate LyC leakers tend to have lower Hα EW than typical for HAEs with that particular UV slope (IDs 8760 and 8954 do not), which qualitatively would agree with the predictions from Zackrisson et al. (2013). However, we note that there is a large spread between Hα EW and UV slope, partly because UV slopes are measured with ground based imaging.

Table 2. Stacked measurements for subsamples of HAEs and LAEs at $z = 2.2$. # indicates the number of objects in each subsample. We further show the general characteristics of the subsample with observed Hα luminosity (corrected for [N II] contribution, see §2.1.2), the Hα extinction with the E($B − V$) value and a Calzetti law, the median stellar mass and UV slope (β) inferred from $V − R$ colours. The NUV column shows the limits on the NUV magnitude. L$_{1500}$ is the rest-frame 1500 Å luminosity obtained from the V band. The absolute f$_{esc}$ is measured from Hα and the NUV as described in §4.1. f$_{esc,rel}$ is the relative escape fraction of ionizing photons to UV photons and is measured from NUV and L$_{1500}$. Note that with a Calzetti law A$_{UV} = 3.1$A$_{H\alpha}$. CLEAN subsamples are samples without foreground/neighbouring source within the NUV PSF (2.7″).

Subsample	#	$\mathbf{L_{H\alpha,obs}}$ erg s^{-1}	$\mathbf{A_{H\alpha}}$ mag	β	$\mathbf{M_{star}}$ $\log_{10}(M_\odot)$	**NUV** 1σ AB	$\mathbf{L_{1500}}$ erg s^{-1}Hz^{-1}	$\mathbf{f_{esc}}$ %	$\mathbf{f_{esc}^{rel}}$ %
Median stacking									
COSMOS HAEs	588	1.56×10^{42}	1.23	-1.89	9.7	30.3	5.04×10^{28}	< 3.4	< 61.7
COSMOS no AGN	578	1.54×10^{42}	1.23	-1.89	9.7	30.3	5.01×10^{28}	< 3.3	< 59.7
COSMOS no AGN CLEAN	191	1.60×10^{42}	1.23	-1.97	9.7	29.7	5.78×10^{28}	< 5.5	< 92.5
Mean stacking									
COSMOS HAEs	588					28.1		< 21.6	< 475.7
−5σ clip						28.7		< 13.8	< 274.7
COSMOS no AGN	578					28.1		< 21.7	< 478.5
−5σ clip						28.7		< 13.8	< 276.2
COSMOS no AGN CLEAN	191					27.9		< 22.7	< 465.4
−5σ clip						28.7		< 12.7	< 231.0

4.3 Stacks of HAEs

The majority of our sources are undetected in the NUV imaging, which is not surprising since the median upper limit on f$_{esc}$ for individual sources is ≈ 60 %. In order to reach more stringent constraints on f$_{esc}$ for typical star-forming galaxies, we stack NUV thumbnails of our full sample of HAEs in COSMOS and also stack various subsets. We create thumbnails of $40'' \times 40''$ centered on the position of the NB$_K$ (Hα) detection and stack these by either median or mean combining the counts in each pixel. While median stacking results in optimal noise properties and is not dominated by outliers, it assumes that the underlying population is uniform, which is likely not the case (particularly if our candidate LyC leakers with high f$_{esc}$ are real; see also the high f$_{esc}$ of the source from Vanzella et al. 2016). Mean stacking is much more sensitive to outliers (such as for example luminous AGN), but would give a more meaningful result as it gives the average f$_{esc}$, which is the important quantity in assessing the ionizing photon output of the entire galaxy population.

We measure the depth by randomly placing 100,000 empty apertures with a radius of 0.67×PSF-FWHM (similar to e.g. Cowie et al. 2009; Rutkowski et al. 2016) in a box of $24'' \times 24''$ around the centre of the thumbnail and quote the 1σ standard deviation as the depth. Apertures with a detection of $NUV < 26$ AB magnitude are masked (this is particularly important for mean stacking). Counts are converted to AB magnitudes with the photometric zero-point of 20.08 (Cowie et al. 2009). For mean stacking, we experiment with an iterative 5σ clipping method in order to have the background not dominated by a few luminous sources. To do this, we compute the standard deviation of the counts of the stacked sample in each pixel and ignore 5σ outliers in computing the mean value of each pixel. This is iterated five times, although we note that most of the mean values already converge after a single iteration.

We first stack the entire sample of HAEs, without removing AGN or sources which are not in the CLEAN subsample. By visual inspection, none of our stacks shows a convincing detection in the NUV filter. As seen in Table 2, we measure a depth of ≈ 30.3 for the median stack of all HAEs. Removing AGN from our sample has little effect, as we have identified only 10 AGN. For our full sample of HAEs, stacking results in an upper limit on the escape fraction of f$_{esc} < 3.4$ %. The upper limit on the relative escape fraction, f$_{esc,rel}$, is much higher (< 61.7 %). However, if we correct for the dust attenuation with the Calzetti et al. (2000) law, we find A$_{UV} \approx 3.8$ and a dust corrected inferred escape fraction of < 1.9 %, although the additional uncertainty due to this dust correction is large. Mean stacking gives shallower constraints because the noise does not decrease as rapidly by stacking more sources, possibly because of a contribution from faint background or companion sources below the detection limit. This is improved somewhat by our iterative 5σ clipping, which effectively masks out the contribution from bright pixels. Therefore, the mean (5σ clip) stack of all star-forming HAEs results in an upper limit of f$_{esc} < 21.6(13.8)$ %.

Due to the large PSF of the NUV imaging, a possible signal may be suppressed by additional background from nearby sources within the NUV PSF. By stacking only sources from the CLEAN sample, the limiting NUV magnitude of the stack of CLEAN HAEs is $NUV \approx 29.7$ AB (see Table 2), which translates into an upper limit of f$_{esc} < 5.5$ %. Interestingly, the upper limit on f$_{esc}$ for mean stacking decreases (f$_{esc} < 12.7$ % with 5σ clipping). This is because the mean stacking method is more sensitive to additional background from nearby sources which are now masked. We show the stacked thumbnails of this sample in Fig. A2.

We have experimented by stacking subsets of galaxies in bins of stellar mass, SFR and UV magnitude or LAEs, but all result in a non-detection in the NUV, all with weaker upper limits than the stack of CLEAN HAEs.

Table 3. Measurements of $\langle f_{esc} \rangle$, the escape fraction of ionizing photons averaged over the galaxy population at $z \approx 2-5$. Constraints on the IGM emissivity from absorption studies by Becker & Bolton (2013) have been used to infer the global escape fraction. For $z = 2.2$, we have used the Hα luminosity function from Sobral et al. (2013). We have used the analytical formula from Madau & Haardt (2015) to estimate the contribution from quasars to the ionizing emissivity, which assumes that $f_{esc,quasars} = 100$ %. At $z = 3.8$ and $z = 4.9$ we have used the SFR function from Smit et al. (2015).

Sample	Method	$\langle f_{esc} \rangle$
This paper		
HAEs $z = 2.2$	full SFR integration, $A_{H\alpha} = 1.0$	$4.4^{+7.1}_{-2.0}$ %
HAEs $z = 2.2$	SFR > 3 M$_\odot$/yr, $A_{H\alpha} = 1.0$	$6.7^{+10.8}_{-3.1}$ %
HAEs $z = 2.2$	full SFR integration, $A_{H\alpha} = 0.7$	$5.9^{+9.3}_{-2.6}$ %
HAEs $z = 2.2$	full SFR integration, $A_{H\alpha} = 1.0$, QSO contribution	$0.5^{+2.3}_{-0.5}$ %
LBGs $z = 3.8$	full SFR integration, Hα from *Spitzer*/IRAC	$2.7^{+5.1}_{-1.6}$ %
LBGs $z = 3.8$	full SFR integration, Hα from *Spitzer*/IRAC, QSO contribution	$0.0^{+2.1}_{-0.0}$ %
LBGs $z = 4.9$	full SFR integration, Hα from *Spitzer*/IRAC	$6.0^{+9.8}_{-3.7}$ %
LBGs $z = 4.9$	full SFR integration, Hα from *Spitzer*/IRAC, QSO contribution	$2.1^{+4.4}_{-1.7}$ %
Literature		
Cristiani et al. (2016) $z = 3.8$	integrated LBG LF + contribution from QSOs	$5.3^{+2.7}_{-1.2}$ %

4.4 Dependence on systematics

4.4.1 Dust

In this sub-section, we investigate how sensitive our results are to the method used to correct for dust. In Table 2, we have used the SED inferred value of E($B - V$) to infer $A_{H\alpha}$: $A_{H\alpha} = E(B - V) \times k_{H\alpha}$, where $k_{H\alpha} = 3.3277$ following Calzetti et al. (2000), which results in $A_{H\alpha} = 1.23$. However, it is also possible to infer $A_{H\alpha}$ from a relation with the UV slope (e.g. Meurer et al. 1999), such that $A_{H\alpha} = 0.641(\beta + 2.23)$, for $\beta > -2.23$ and $A_{H\alpha} = 0$ for $\beta < -2.23$. Finally, we also use the relation between $A_{H\alpha}$ and stellar mass from Garn & Best (2010), which is: $A_{H\alpha} = 0.91 + 0.77X + 0.11X^2 - 0.09X^3$, where $X = \log_{10}(M_{star}/10^{10}$ M$_\odot$). Note that we assume a Calzetti et al. (2000) dust law in all these prescriptions.

It is immediately clear that there is a large systematic uncertainty in the dust correction, as for our full sample of HAEs we infer $A_{H\alpha} = 0.70$ with the Garn & Best (2010) prescription and $A_{H\alpha} = 0.19$ following Meurer et al. (1999), meaning that the systematic uncertainty due to dust can be as large as a factor 3. Thus, these different dust corrections result in different upper limits on f_{esc}. For the CLEAN, star-forming HAE sample, the upper limit on f_{esc} from median stacking increases to $f_{esc} < 8.8\,(13.3)$ %, using the attenuation based on stellar mass (β). With a simple 1 magnitude of extinction for Hα, $f_{esc} < 6.8$ %.

4.4.2 Other systematic errors

In addition to the dust correction, additional systematic uncertainties lie in the parameters ϵ, $c_{H\alpha}$ and T_{IGM} (see Equations 2-6).

The ϵ parameter, which is the mean photon energy convolved over the *NUV* filter may increase with decreasing metallicity or if rotating stars (e.g. Leitherer et al. 2014) or binary stars (e.g. Stanway et al. 2016) are taken into account. However, this increase ϵ is conservatively still within 10%. This is similar to the uncertainty on $c_{H\alpha}$, the recombination coefficient of the Hα line, which depends only modestly on the density and the temperature. For example, in the case of a temperature of T = 30000 K, $c_{H\alpha}$ decreases only by $\approx 10\%$ (Schaerer 2002).

For individual sources (and thus different sight-lines through the IGM) T_{IGM} can vary significantly, e.g. Siana et al. (2007). Particularly, as highlighted by a simulation from Vasei et al. (2016), the mean value of T_{IGM} at $z \approx 2.4$ is not the most common value. The distribution is bimodal, with a narrow peak at $T_{IGM} \approx 0.0$ and a broad peak around $T_{IGM} = 0.7$. Therefore, T_{IGM} is highly uncertain for individual sources, but relatively well constrained within 10 % for statistical samples. For our measurements of f_{esc}, the uncertainties in α are thus maximally of the order 30 % (10 % for each ϵ, $c_{H\alpha}$ and T_{IGM}). This would translate to an uncertainty in f_{esc} of maximally ~ 2 %.

Summarising this section, we find that roughly 5 % of the HAEs are (candidate) LyC leakers, each with escape fractions up to 90 %. However, we find that the escape fraction is low for the typical galaxy, $f_{esc} < 5.5$ % using median stacking. Averaged over the galaxy population, a slightly higher escape fraction is allowed ($f_{esc} < 12.7$ %, clipped mean stacking), which is consistent with a scenario where only a small fraction of galaxies has a relatively high escape fraction.

5 CONSTRAINING F$_{ESC}$ OF HAES FROM THE IONIZING BACKGROUND

In addition to constraining f_{esc} directly, we can obtain an indirect measurement of f_{esc} by using the ionizing emissivity, measured from quasar absorption studies, as a constraint. The emissivity is defined as the number of escaping ionizing photons per second per comoving volume:

$$\dot{N}_{ion} = \langle f_{esc} \rangle \times \Phi(H\alpha) \times c_{H\alpha}^{-1} \qquad (6)$$

Here, $\dot{N}_{ion}$ is in s^{-1} Mpc^{-3}, $\langle f_{esc} \rangle$ is the escape fraction averaged over the entire galaxy population, $\Phi(H\alpha)$ is the Hα luminosity density in erg s^{-1} Mpc^{-3} and $c_{H\alpha}$ is the recombination coefficient as in Eq. 2.

We first check whether our derived emissivity using our upper limit on f_{esc} for HAEs is consistent with published

measurements of the emissivity. The Hα luminosity density is measured in Sobral et al. (2013) as the full integral of the Hα luminosity function, with a global dust correction of $A_{H\alpha} = 1.0$. Using the mean limit on f_{esc} for our CLEAN sample of HAEs (so $f_{esc} \leq 12.7$ %), we find that $\dot{N}_{ion} \leq 2.6^{+0.2}_{-0.2} \times 10^{51}$ s^{-1} Mpc^{-3}, where the errors come from the uncertainty in the Hα LF. We note that these numbers are relatively independent on the dust correction method because while a smaller dust attenuation would decrease the Hα luminosity density, it would also raise the upper limit on the escape fraction, thus almost cancelling out. These upper limits on $\dot{N}_{ion}$ are consistent with the measured emissivity at $z = 2.4$ of Becker & Bolton (2013), who measured $\dot{N}_{ion} = 0.90^{+1.60}_{-0.52} \times 10^{51}$ s^{-1} Mpc^{-3} (combined systematic and measurement errors) using the latest measurements of the IGM temperature and opacity to Lyα and LyC photons.

Now, by isolating $\langle f_{esc} \rangle$ in Eq. 7, we can estimate the globally averaged escape fraction. If we assume that there is no evolution in the emissivity from Becker & Bolton (2013) between $z = 2.2$ and $z = 2.4$ and that the Hα luminosity function captures all sources of ionizing photons, we find that $\langle f_{esc} \rangle = 4.4^{+7.1}_{-2.0}$ % for $A_{H\alpha} = 1.0$. When integrating the Hα LF only to SFR ≈ 3 M$_\odot$ yr^{-1}, $\langle f_{esc} \rangle = 6.7^{+10.8}_{-3.1}$ %. If $A_{H\alpha} = 0.7$, which is the median value when we correct for dust using stellar mass, and which may be more representative of fainter Hα emitters (as faint sources are expected to have less dust), the escape fraction is somewhat higher, with $\langle f_{esc} \rangle = 5.9^{+9.3}_{-2.6}$ %. This relatively small difference is shown by the two red symbols in Fig. 5. These numbers are summarised in Table 3.

We note that an additional contribution to the ionizing emissivity from rarer sources than sources with number densities $< 10^{-5}$ Mpc^{-3} such as quasars, would lower the escape fraction for HAEs. While Madau & Haardt (2015) argue that the ionizing budget at $z \approx 2 - 3$ is dominated by quasars, this measurement may be overestimated by assuming quasars have a 100 % escape fraction. Recently, Micheva et al. (2016) obtained a much lower emissivity (up to a factor of 10) from quasars by directly measuring f_{esc} for a sample of $z \sim 3$ AGN. Using a large sample of quasars at $z = 3.6 - 4.0$, Cristiani et al. (2016), measure a mean $\langle f_{esc,quasar} \rangle \approx 70$ %, which means that quasars do not dominate the ionizing background at $z \approx 4$. When we include a quasar contribution from Madau & Haardt (2015) in the most conservative way (meaning that we assume $f_{esc} = 100$ % for quasars), we find that $\langle f_{esc} \rangle = 0.5^{+2.3}_{-0.5}$ %. If the escape fraction for quasars is 70 %, $\langle f_{esc} \rangle = 1.6^{+3.4}_{-0.8}$ %, such that a non-zero contribution from star-forming galaxies is still required.

These measurements of $\langle f_{esc} \rangle$ contain significantly less (systematic) uncertainties than measurements based on the integral of the UV luminosity function (e.g. Becker & Bolton 2013; Khaire et al. 2016). This is because: i) UV selected galaxy samples do not span the entire range of SFGs (e.g. Oteo et al. 2015) and might thus miss dusty star-forming galaxies and ii) there are additional uncertainties in converting non-ionizing UV luminosity to intrinsic LyC luminosity (in particular the dust corrections in ξ_{ion} and uncertainties in the detailed SED models in $(L_{UV}/L_{NUV})_{int}$). An issue is that Hα is very challenging to observe at $z \gtrsim 2.8$ and that a potential spectroscopic follow-up study of UV selected galaxies with the *JWST* might yield biased results.
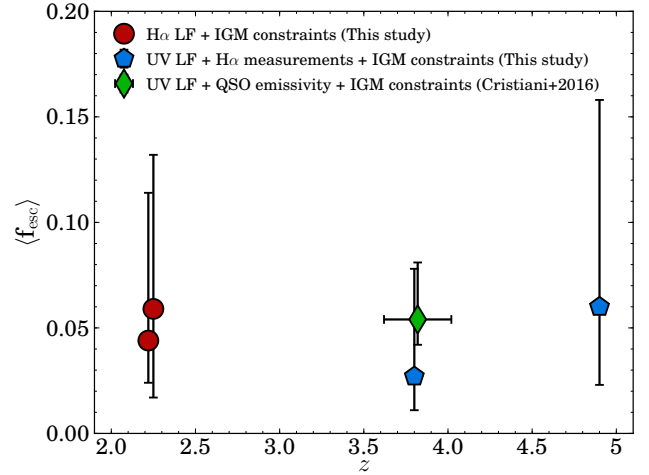

Figure 5. Evolution of the globally averaged $\langle f_{esc} \rangle$, which is obtained by forcing the emissivity of the integrated Hα ($z = 2.2$) and UV ($z \approx 4 - 5$) LF to be equal to the emissivity measured by IGM absorption models from Becker & Bolton 2013. The $z \approx 4 - 5$ results are based on a UV luminosity function which is then corrected to a SFR function with Hα measurements from *Spitzer*/IRAC, which implicitly means using a value of ξ_{ion} (SFR functions are presented in Smit et al. 2015, but see also Bouwens et al. 2016). The different, slightly shifted red symbols indicate that the globally averaged f_{esc} depends only little on the method used to correct for dust (see text). Integrating to SFR> 3M$_\odot$/yr instead of fully integrating the SFR function results in a factor ≈ 1.5 higher $\langle f_{esc} \rangle$. The green diamond shows the estimated value by Cristiani et al. 2016, who combined IGM constraints with a UV LBG and the emissivity of QSOs at $z = 3.6 - 4.0$.

5.1 Redshift evolution

Using the same methodology as described in §5, we also compute the average f_{esc} at $z = 3.8$ and $z = 4.9$ by using the SFR functions of Smit et al. (2015), which are derived from UV luminosity functions, a Meurer et al. (1999) dust correction and a general offset to correct for the difference between SFR(UV) and SFR(Hα), estimated from *Spitzer*/IRAC photometry. This offset is implicitly related to the value of ξ_{ion} from Bouwens et al. (2016), which is estimated from the same measurements. We combine these SFR functions, converted to the Hα luminosity function as in §2.1.2, with the IGM emissivity from Becker & Bolton (2013) at $z = 4.0$ and $z = 4.75$, respectively. Similarly to the Hα luminosity density, we use the analytical integral of the Schechter function. This results in $\langle f_{esc} \rangle = 2.7^{+5.1}_{-1.6}$ % and $\langle f_{esc} \rangle = 6.0^{+9.8}_{-3.7}$ % at $z \approx 4$ and $z \approx 5$, respectively, see Table 3. When including a (maximum) quasar contribution from Madau & Haardt (2015) as described above, we find $\langle f_{esc} \rangle = 0.0^{+2.1}_{-0.0}$ % at $z \approx 4$ and $\langle f_{esc} \rangle = 2.1^{+4.4}_{-1.7}$ %.

As illustrated in Fig. 5, the global escape fraction is relatively constant (and low) between $z \approx 2 - 5$. While dust has been corrected for with different methods at $z = 2.2$ and $z \approx 4 - 5$, we note that the differences between different dust correction methods are not expected to be very large at $z \approx 4 - 5$. This is because higher redshift galaxies typically are of lower mass, which results in a higher agreement between dust correction methods based on either M$_{star}$ or β.

One potentially important caveat is that our computation assumes that the Hα and UV luminosity functions include all sources of ionizing photons in addition to quasars. An additional contribution of ionizing photons from galaxies which have potentially been missed by a UV selection (for example sub-mm galaxies) would decrease the global f_{esc}. Such a bias is likely more important at $z \approx 3-5$ than $z \approx 2$ because the $z \approx 2$ sample is selected with Hα which is able to recover sub-mm galaxies. Even under current uncertainties, we rule out a globally averaged $\langle f_{esc} \rangle > 20$ % at redshifts lower than $z \approx 5$.

These indirectly derived escape fractions of ~ 4 % at $z \approx 2-5$ are consistent with recently published upper limits from Sandberg et al. (2015) at $z = 2.2$ and similar to strict upper limits on f_{esc} at $z \sim 1$ measured by Rutkowski et al. (2016). Recently, Cristiani et al. (2016) estimated that galaxies have on average $\langle f_{esc} \rangle = 5.3^{+2.7}_{-1.2}$ % at $z \approx 4$ by combining IGM constraints with the UV luminosity function from Bouwens et al. (2011) and by including the contribution from quasars to the total emissivity. This result is still consistent within the error-bars with our estimate using the Madau & Haardt (2015) quasar contribution and Smit et al. (2015) SFR function. Part of this is because we use a different conversion from UV luminosity to the number of produced ionizing photons based on Hα estimates with *Spitzer*/IRAC, and because our computation assumes $f_{esc,quasars} = 100\%$, while Cristiani et al. (2016) uses $f_{esc,quasars} \approx 70\%$.

Furthermore, our results are also consistent with observations from Chen et al. (2007) who find a mean escape fraction of 2 ± 2 % averaged over galaxy viewing angles using spectroscopy of the afterglow of a sample of γ-Ray bursts at $z > 2$. Grazian et al. (2016) measures a strict median upper limit of $f_{esc}^{rel} < 2$ % at $z = 3.3$, although this limit is for relatively luminous Lyman-break galaxies and not for the entire population of SFGs. This would potentially indicate that the majority of LyC photons escape from galaxies with lower luminosity, or galaxies missed by a Lyman-break selection, c.f. Cooke et al. (2014) or that they come from just a sub-set of the population, and thus the median f_{esc} can even be close to zero. Khaire et al. (2016) finds that f_{esc} must evolve from $\approx 5-20$ % between $z = 3-5$, which is in tension with our measurement at $z \approx 5$. However, part of this tension may be caused by their assumption that the number of produced ionizing photons per unit UV luminosity does not evolve with redshift. In §6.5 we find that there is evolution of this number by roughly a factor 1.5, such that the required evolution of f_{esc} would only be a factor ≈ 3, which is allowed within our error-bars. While our results indicate little to no evolution in the average escape fraction up to $z \approx 5$, this does not rule out an increasing f_{esc} at $z > 5$, where theoretical models expect an evolving f_{esc} (e.g. Kuhlen & Faucher-Giguère 2012; Ferrara & Loeb 2013; Mitra et al. 2013; Khaire et al. 2016; Sharma et al. 2016; Price et al. 2016), see also a recent observational claim of evolving f_{esc} with redshift (Smith et al. 2016).

Finally, we stress that a low $\langle f_{esc} \rangle$ is not inconsistent with the recent detection of the high f_{esc} of above 50 % from a galaxy at $z \approx 3$ (De Barros et al. 2016; Vanzella et al. 2016), which may simply reflect that there is a broad distribution of escape fractions. We note that if indeed 5 % of our galaxies are confirmed as LyC leakers with $f_{esc} \approx 75$ %, the average f_{esc} over the galaxy population is ≈ 4 %,
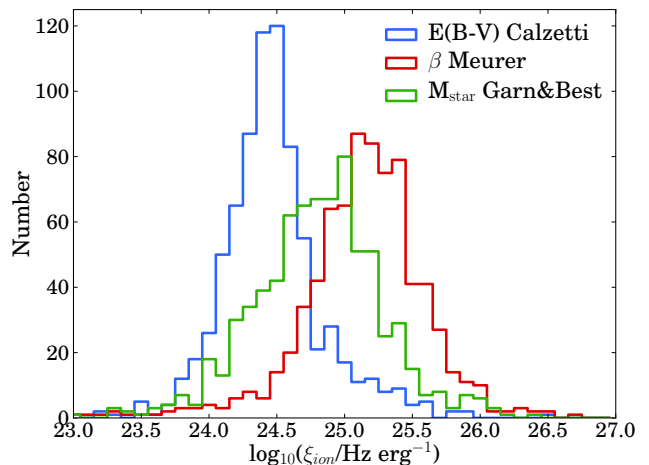

Figure 6. Histogram of the values of ξ_{ion} for HAEs with three different methods to correct for dust attenuation. The blue histogram shows values of ξ_{ion} when dust is corrected with the $E(B-V)$ value from the SED in combination with a Calzetti law (see §2.1). The red histogram is corrected for dust with the Meurer et al. 1999 prescription based on the UV slope and the green histogram is corrected for dust with the prescription from Garn & Best 2010 based on a relation between dust attenuation and stellar mass. As can be seen, the measured values of ξ_{ion} differ significantly, with the highest values found when correcting for dust with the UV slope. When the nebular attenuation is higher than the stellar attenuation, ξ_{ion} would shift to higher values.

consistent with the indirect measurement, even if $f_{esc} = 0$ for all other galaxies. Such a scenario would be the case if the escape of LyC photons is a very stochastic process, for example if it is highly direction or time dependent. This can be tested with deeper LyC limits on individual galaxies.

6   THE IONIZING PROPERTIES OF STAR-FORMING GALAXIES AT $Z = 2.2$

6.1   How to measure ξ_{ion}?

The number of ionizing photons produced per unit UV luminosity, ξ_{ion}, is used to convert the observed UV luminosity of high-redshift galaxies to the number of produced ionizing photons. ξ_{ion} can be measured from the ratio of dust corrected Hα luminosity and UV luminosity, as the Hα luminosity traces the number of ionizing photons. Therefore, ξ_{ion} is defined as:

$$\xi_{ion} = Q_{ion}/L_{UV,int} \qquad (7)$$

As described in the previous section, Q_{ion} (in s^{-1}) can be measured directly from the dust-corrected Hα luminosity by rewriting Eq. 2 and assuming $f_{esc} = 0$. $L_{UV,int}$ (in erg s^{-1} Hz^{-1}) is obtained by correcting the observed UV magnitudes for dust attenuation. With a Calzetti et al. (2000) attenuation curve $A_{UV} = 3.1A_{H\alpha}$.

6.2 ξ_{ion} at $z = 2.2$

We show our measured values of ξ_{ion} for HAEs in Fig. 6 and Table 4, where dust attenuation is corrected with three
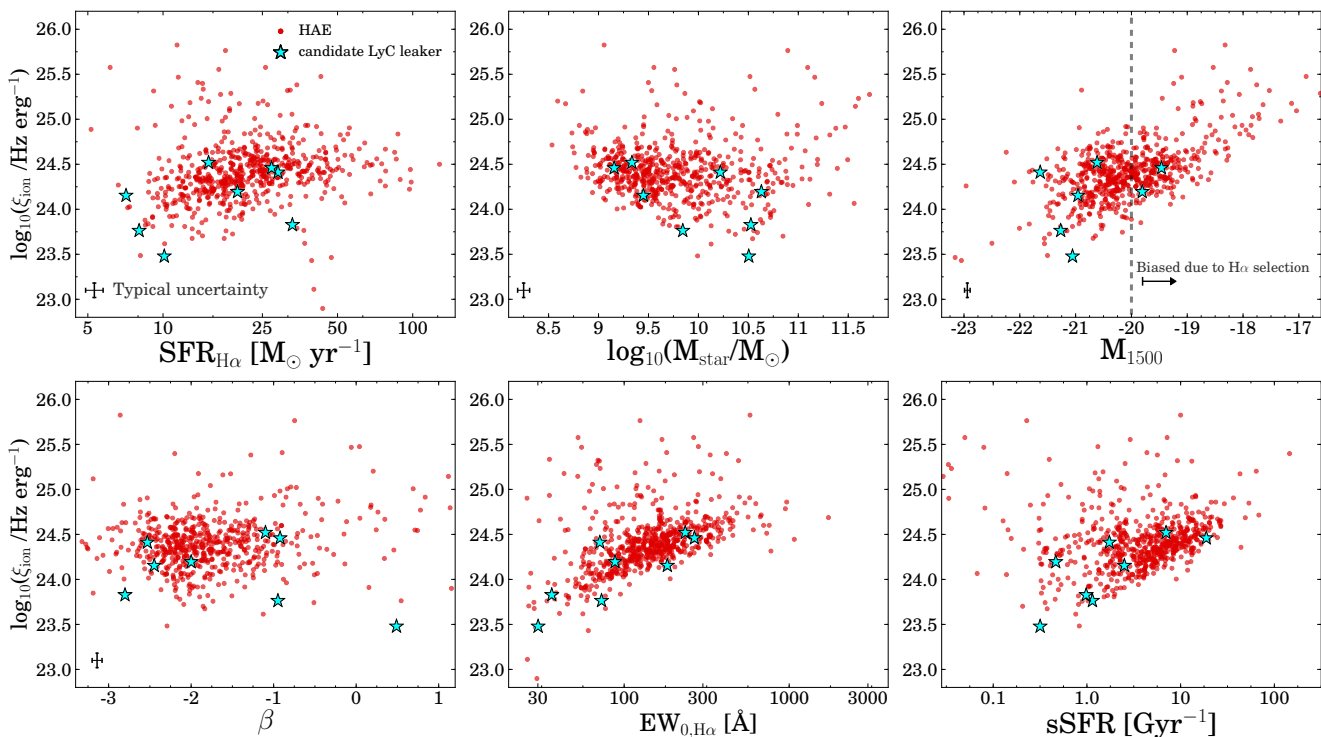
Figure 7. Correlations between ξ_{ion} and galaxy properties for HAEs, when dust is corrected using the SED fitted E$(B - V)$ values. Red symbols show HAEs and candidate LyC leakers are indicated with a cyan star. ξ_{ion} does not clearly correlate with SFR(Hα), M$_{star}$ or β. A correlation between ξ_{ion} and M$_{1500}$ is expected of similar strength as seen, based on the definition of ξ_{ion}. ξ_{ion} increases strongly with Hα EW and sSFR. High values of ξ_{ion} at low sSFRs are mostly due to the dust correction.

different methods based either on the E$(B - V)$ value of the SED fit, the UV slope β or the stellar mass. It can be seen that the average value of ξ_{ion} is very sensitive to the dust correction method, as it ranges from $\xi_{ion} = 10^{24.39 \pm 0.04}$ Hz erg^{-1} for the SED method to $\xi_{ion} = 10^{25.11 \pm 0.04}$ Hz erg^{-1} for the β method. For the dust correction based on stellar mass the value lies in between, with $\xi_{ion} = 10^{24.77 \pm 0.04}$ Hz erg^{-1}. In the case of a higher nebular attenuation than the stellar attenuation, as for example by a factor ≈ 2 as in the original Calzetti et al. (2000) prescription, ξ_{ion} increases by 0.4 dex to $\xi_{ion} = 10^{24.79 \pm 0.04}$ Hz erg^{-1} when correcting for dust with the SED fit.

We note that independent measurements of the dust attenuation from *Herschel* and Balmer decrements at $z \sim 1 - 2$ indicate that dust attenuations agree very well with the Garn & Best (2010) prescription (e.g. Sobral et al. 2012; Ibar et al. 2013; Buat et al. 2015; Pannella et al. 2015), thus favouring the intermediate value of ξ_{ion}. Without correcting ξ_{ion} for dust, we find $\xi_{ion} = 10^{25.41 \pm 0.05}$ Hz erg^{-1}. With 1 magnitude of extinction for Hα, as for example used in the conversion of the Hα luminosity density to a SFR density in Sobral et al. (2013), $\xi_{ion} = 10^{24.57 \pm 0.04}$ Hz erg^{-1}.

Since individual Hα measurements for LAEs are uncertain due to the difference in filter transmissions depending on the particular redshift (see Matthee et al. 2016), we only investigate ξ_{ion} for our sample of LAEs in the stacks which are described in Sobral et al. (2016a). As seen in Table 4, the median ξ_{ion} is higher than the median ξ_{ion} for HAEs for each dust correction. However, this difference disappears

without correcting for dust. Therefore, the lower values of ξ_{ion} for LAEs simply indicate that the median LAE has a bluer UV slope, lower stellar mass and lower E$(B - V)$ than the median HAE. More accurate dust measurements are required to investigate whether ξ_{ion} is really higher for LAEs. We note that ≈ 40 % of the LAEs are undetected in the broad-bands and thus assigned a stellar mass of 10^8 M$_\odot$ and E$(B - V) = 0.1$ when computing the median dust attenuation. Therefore, the ξ_{ion} values for LAEs could be under-estimated if the real dust attenuation is even lower.

6.3 Dependence on galaxy properties

In this section we investigate how ξ_{ion} depends on the galaxy properties that are defined in §2.1 and also check whether subsets of galaxies lie in a specific parameter space. As illustrated in Fig. 7 (where we correct for dust with E$(B - V)$), we find that ξ_{ion} does not depend strongly on SFR(Hα) with a Spearman correlation rank (R$_s$) of R$_s = 0.11$. Such a correlation would naively be expected if the Hα SFRs are not related closely to UV SFRs, since $\xi_{ion} \propto L_{H\alpha}/L_{1500} \propto$ SFR(Hα)/SFR(UV). However, for our sample of galaxies these SFRs are strongly correlated with only 0.3 dex of scatter, see also Oteo et al. (2015), leading to a relatively constant ξ_{ion} with SFR.

For the same reason, we measure a relatively weak slope of ≈ 0.25 when we fit a simple linear relation between $\log_{10}(\xi_{ion})$ and M$_{1500}$, instead of the naively expected value of $\xi_{ion} \propto 0.4 M_{1500}$. At M$_{1500} > -20$, our H$\alpha$ selection is
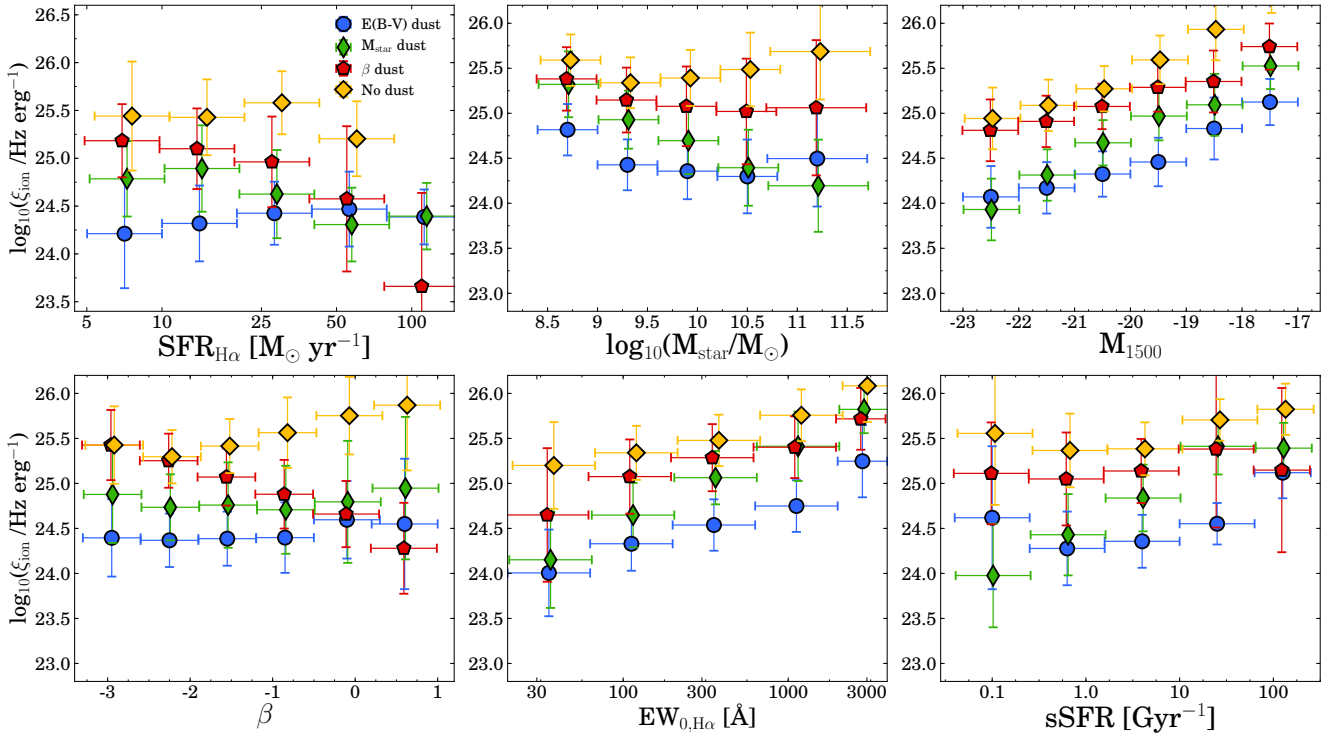
Figure 8. Correlations between ξ_{ion} and galaxy properties for different methods to correct for dust attenuation. To facilitate the comparison, HAEs were binned on the x-axis. The value of ξ_{ion} is the median value in each bin, while the vertical error is the standard deviation. Blue bins show the values where dust is corrected with the E$(B-V)$ value from the SED. The red bins are corrected for dust with the Meurer et al. (1999) prescription based on β and the green bins are corrected for dust with the prescription from Garn & Best (2010) based on stellar mass. Yellow bins show the results where we assume that there is no dust.

biased towards high values of Hα relative to the UV, leading to a bias in high values of ξ_{ion} (see Fig. 4). For sources with $M_{1500} < -20$, we measure a slope of ≈ 0.2. This means that ξ_{ion} does not increase rapidly with decreasing UV luminosity. This is because Hα luminosity and dust attenuation themselves are also related to M_{1500}. Indeed, we find that the Hα luminosity anti-correlates with the UV magnitude and E$(B-V)$ increases for fainter UV magnitudes.

The stellar mass and β are not by definition directly related to ξ_{ion}. Therefore, a possible upturn of ξ_{ion} at low masses (see the middle-top panel in Fig. 7) may be a real physical effect, although we note that we are not mass-complete below $M_{star} < 10^{10}$ $M_\odot$ and an Hα selected sample of galaxies likely misses low-mass galaxies with lower values of ξ_{ion}.

We find that the number of ionizing photons per unit UV luminosity is strongly related to the Hα EW (with a slope of ~ 0.6 in log-log space), see Fig. 7. Such a correlation is expected because of our definition of ξ_{ion}: i) the Hα EW increases mildly with increasing Hα (line-)luminosity and ii) the Hα EW is weakly anti-related with the UV (continuum) luminosity, such that ξ_{ion} increases relatively strongly with EW. Since there is a relation between Hα EW and specific SFR (sSFR = SFR/M_{star}, e.g. Fumagalli et al. 2012), we also find that ξ_{ion} increases strongly with increasing sSFR, see Fig. 7.

In Fig. 8 we show the same correlations as discussed above, but now compare the results for different methods to

correct for dust. For comparison, we only show the median ξ_{ion} in bins of the property on the x-axis. The vertical error on the bins is the standard deviation of the values of ξ_{ion} in the bin. As ξ_{ion} depends on the dust correction, we find that ξ_{ion} correlates with the galaxy property that was used to correct for dust in the case of β (red symbols) and M_{star} (green symbols). Specific SFR depends on stellar mass, so we also find the strongest correlation between sSFR and ξ_{ion} when ξ_{ion} is corrected for dust with the Garn & Best (2010) prescription. We only find a relation between ξ_{ion} and β when dust is corrected with the Meurer et al. (1999) prescription. For UV magnitude only the normalisation of ξ_{ion} changes with the dust correction method.

It is more interesting to look at correlations between ξ_{ion} and galaxy properties which are not directly related to the computation of ξ_{ion} or the dust correction. Hence, we note that irrespective of the dust correction method, ξ_{ion} appears to be somewhat higher for lower mass galaxies (although this is likely a selection effect as discussed above). Irrespective of the dust correction method, ξ_{ion} increases with increasing Hα EW and fainter M_{1500}, where the particular dust correction method used only sets the normalisation. We return to this relation between ξ_{ion} and Hα EW in §6.5.

6.4   Dependence on systematics

In our definition of ξ_{ion}, we have assumed that the escape fraction of ionizing photons is ≈ 0. Our direct con-

Table 4. ionizing properties of HAEs and LAEs for various methods to correct for dust attenuations and different subsets. We show the median stellar mass of each subsample. Errors on ξ_{ion} are computed as $\sigma_{\xi_{ion}}/\sqrt{N}$, where $\sigma_{\xi_{ion}}$ is the median measurement error of ξ_{ion} and N the number of sources. For the Bouwens et al. (2016) measurements, we show only dust corrections with Calzetti et al. (2000) curve. The subsample of 'low mass' HAEs has $M_{star} = 10^{9-9.4}$ $M_{\odot}$. 'UV faint' HAEs have $M_{1500} > -19$.

Sample	$<M_{star}>$ $\log_{10}$ $M_{\odot}$	$\log_{10}$ ξ_{ion} Hz erg^{-1}	Dust
This paper			
HAEs $z = 2.2$	9.8	24.39 ± 0.04	$E(B-V)$
		25.11 ± 0.04	β
		24.77 ± 0.04	M_{star}
		25.41 ± 0.05	No dust
		24.57 ± 0.04	$A_{H\alpha} = 1$
Low mass	9.2	24.49 ± 0.06	$E(B-V)$
		25.22 ± 0.06	β
		24.99 ± 0.06	M_{star}
UV faint	10.2	24.93 ± 0.07	$E(B-V)$
		25.39 ± 0.07	β
		25.24 ± 0.07	M_{star}
LAEs $z = 2.2$	8.5	24.84 ± 0.09	$E(B-V)$
		25.37 ± 0.09	β
		25.14 ± 0.09	M_{star}
		25.39 ± 0.09	No dust
Bouwens et al. (2016)			
LBGs $z = 3.8 - 5.0$	9.2	25.27 ± 0.03	β
LBGs $z = 5.1 - 5.4$	9.2	25.44 ± 0.12	β

straint of $f_{esc} \lesssim 10\%$ and our indirect global measurement of $f_{esc} \approx 4 - 5$ % validate this assumption. If the average is $f_{esc} = 10\%$, ξ_{ion} is higher by a factor 1.11 (so only 0.04 dex). For individual candidate LyC leakers, f_{esc} may be significantly higher, even 90%. In that case, ξ_{ion} may be underestimated by a factor of 10. We have marked the candidate LyC leakers in Fig. 7 in order to check whether they are positioned in a particular part of parameter space (and thus could bias trends between ξ_{ion} and galaxy properties). We find no such bias, except for potentially higher f_{esc} at low Hα SFRs (which is not surprising, since the Hα luminosity scales with $1 - f_{esc}$).

6.5 Redshift evolution of ξ_{ion}

Because of its dependency on galaxy properties, it is possible that ξ_{ion} evolves with redshift. In fact, such an evolution is expected as more evolved galaxies (particularly with declining star formation histories) have a relatively stronger UV luminosity than Hα and a higher dust content, likely leading to a lower ξ_{ion} at $z = 2.2$ than at $z > 6$.

By comparing our measurement of ξ_{ion} with those from Bouwens et al. (2016), we already find such an evolution (see Table 4), although we note that the samples of galaxies are selected differently and that there are many other differences, such as the dust attenuation, typical stellar mass and the Hα measurement. If we mimic a Lyman-break selected sample by only selecting HAEs with $E(B-V) < 0.3$ (typical for UV selected galaxies, e.g. Steidel et al. 2011), we find that ξ_{ion} increases by (maximally) 0.1 dex, such that this does likely not explain the difference in ξ_{ion} at $z = 2.2$ and

Table 5. Fit parameters for $\log_{10} \xi_{ion} = a + b \log_{10}$ EW(Hα) for different selections and dust corrections

Sample	$<M_{star}>$ $\log_{10}$ $M_{\odot}$	a	b	Dust
All HAEs	9.8	23.12	0.59	$E(B-V)$
		23.66	0.64	β
		22.60	0.97	M_{star}
		23.59	0.45	$A_{H\alpha} = 1$
Low mass	9.2	22.64	0.78	$E(B-V)$
		23.68	0.64	β
		23.19	0.77	M_{star}
		22.77	0.75	$A_{H\alpha} = 1$

$z \approx 4 - 5$ of ≈ 0.5 dex. Furthermore, as illustrated in Fig. 4 our Hα selection actually is biased towards high values of ξ_{ion} for $M_{1500} > -20$, which likely mitigates the difference on the median ξ_{ion}. If we select only low mass galaxies such that the median stellar mass resembles that of Bouwens et al. (2016), the difference is only $\approx 0.2 \pm 0.1$ dex, which still would suggest evolution.

We estimate the redshift evolution of ξ_{ion} by combining the relation between ξ_{ion} and Hα EW with the redshift evolution of the Hα EW. Several studies have recently noted that the Hα EW (and related sSFR) increases with increasing redshift (e.g. Fumagalli et al. 2012; Sobral et al. 2014; Smit et al. 2014; Marmol-Queralto et al. 2015; Faisst et al. 2016; Khostovan et al. 2016). Furthermore, the EW is mildly dependent on stellar mass as EW $\sim M_{star}^{-0.25}$ (Sobral et al. 2014; Marmol-Queralto et al. 2015). In order to estimate the ξ_{ion} using the Hα EW evolution, we:

i) Select a subset of our HAEs with stellar mass between $10^{9-9.4}$ $M_{\odot}$, with a median of $M_{star} \approx 10^{9.2}$ $M_{\odot}$, which is similar to the mass of the sample from Bouwens et al. (2016), see Smit et al. (2015),

ii) Fit a linear trend between $\log_{10}$(EW) and $\log_{10}(\xi_{ion})$ (with the Garn & Best (2010) prescription to correct for dust attenuation). We note that the trend between EW and ξ_{ion} will be steepened if dust is corrected with a prescription based on stellar mass (since Hα EW anti-correlates with stellar mass, see also Table 5). However, this is validated by several independent observations from either Herschel or Balmer decrements which confirm that dust attenuation increases with stellar mass at a wide range of redshifts (Domínguez et al. 2013; Buat et al. 2015; Koyama et al. 2015; Pannella et al. 2015; Sobral et al. 2016b).

Using a simple least squares algorithm, we find:

$$\log_{10}(\xi_{ion}) = 23.19^{+0.09}_{-0.09} + 0.77^{+0.04}_{-0.04} \times \log_{10}(\text{EW}) \quad (8)$$

iii) Combine the trend between Hα EW and redshift with the trend between ξ_{ion} and Hα EW. We use the redshift evolution of the Hα EW from Faisst et al. (2016), which has been inferred from fitting SEDs, and measured up to $z \approx 6$. In this parametrisation, the slope changes from EW$\approx (1 + z)^{1.87}$ at $z < 2.2$ to EW$\approx (1 + z)^{1.3}$ at $z > 2.2$. Below $z < 2.2$, this trend is fully consistent with the EW evolution from HiZELS (Sobral et al. 2014), which is measured with narrow-band imaging. Although HiZELS does not have Hα emitters at $z > 2.2$, the EW evolution of [OIII]+Hβ is found to flatten at $z > 2.2$ as well (Khostovan et al. 2016). We note that we assume that the slope of the Hα EW evolution with
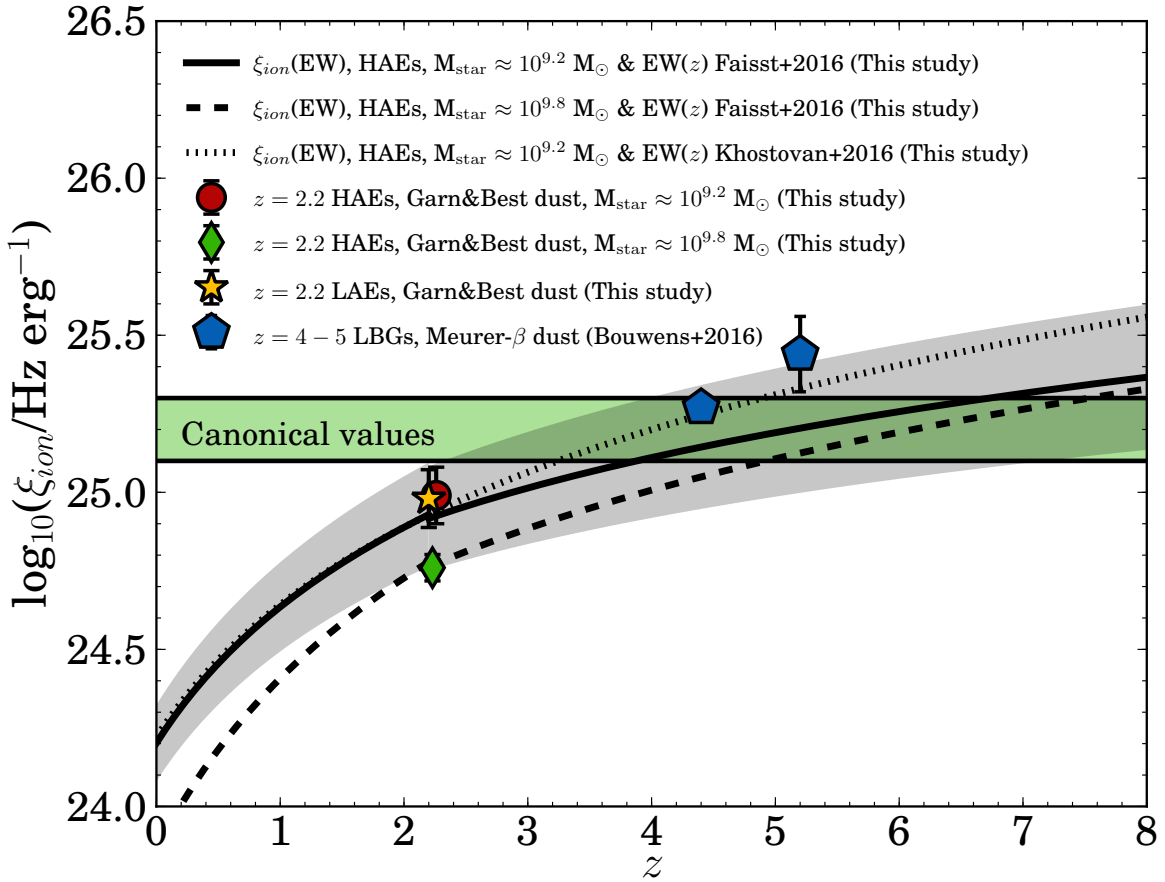
Figure 9. Inferred evolution of ξ_{ion} (corrected for dust with M_{star}) with redshift based on our observed trend between ξ_{ion} and Hα EW, for different stellar massess (compare the solid with the dashed line) and EW(z) evolutions (compare the solid with the dotted line). The grey shaded region indicates the errors on the redshift evolution of ξ_{ion}. The normalisation of ξ_{ion} is higher for lower mass galaxies or LAEs. The green region shows the typically assumed values. The estimated evolution of ξ_{ion} with redshift is consistent with the typically assumed values of ξ_{ion} in the reionization era and with recent measurements at $z = 4 - 5$.

redshift does not vary strongly for stellar masses between $10^{9.2}$ M$_\odot$ and $10^{9.8}$ M$_\odot$, since the following equations are measured at stellar mass $\approx 10^{9.6}$ M$_\odot$ (Faisst et al. 2016), hence:

$$\text{EW}(z) = \begin{cases} 20 \times (1+z)^{1.87}, & z < 2.2 \\ 37.4 \times (1+z)^{1.3}, & z \geq 2.2 \end{cases} \quad (9)$$

This results in:

$$\log_{10}(\xi_{ion}(z)) = \begin{cases} 24.19 + 1.44 \times \log_{10}(1+z), & z < 2.2 \\ 24.40 + 1.00 \times \log_{10}(1+z), & z \geq 2.2 \end{cases} \quad (10)$$

where ξ_{ion} is in Hz erg^{-1}. The error on the normalisation is 0.09 Hz erg^{-1} and the error on the slope is 0.18. For our typical mass of $M_{star} = 10^{9.8}$ M$_\odot$, the normalisation is roughly 0.2 dex lower and the slope a factor ≈ 1.1 higher compared to the fit at lower stellar masses. This is due to a slightly different relation between ξ_{ion} and EW (see Table 5). The evolving ξ_{ion} is consistent with the typically assumed value of $\xi_{ion} = 10^{25.2 \pm 0.1}$ Hz erg^{-1} (e.g. Robertson et al. 2013) at $z \approx 2.5 - 12$ within the 1σ error bars.

We show the inferred evolution of ξ_{ion} with redshift

in Fig. 9. The solid and dashed line use the EW(z) evolution from Faisst et al. (2016), while the dotted line uses the Khostovan et al. (2016) parametrisation. The grey shaded region indicates the errors on the redshift evolution of ξ_{ion}. Due to the anti-correlation between EW and stellar mass, galaxies with a lower stellar mass have a higher ξ_{ion} (which is then even strengthened by a higher dust attenuation at high masses).

Relatively independent of the dust correction (as discussed in Fig. *B1*), the median ξ_{ion} increases ≈ 0.2 dex at fixed stellar mass between $z = 2.2$ and $z = 4.5$. This can easily explain the 0.2 dex difference between our measurement at $z = 2.2$ and the Bouwens et al. (2016) measurements at $z = 4 - 5$ (see Fig. 9), such that it is plausible that ξ_{ion} evolves to higher values in the reionization epoch, of roughly $\xi_{ion} \approx 10^{25.4}$ Hz erg^{-1} at $z \approx 8$.

7   IMPLICATIONS FOR REIONIZATION

The product of $f_{esc}\xi_{ion}$ is an important parameter in assessing whether galaxies have provided the photons to reionize the Universe, because these convert the (non-ionizing)

UV luminosity density (obtained from integrating the dust-corrected UV luminosity function) to the ionizing emissivity. The typical adopted values are $\xi_{ion} \approx 10^{25.2-25.3}$ Hz erg^{-1} and f$_{esc} \approx 0.1 - 0.2$ (e.g. Robertson et al. 2015), such that the product is $f_{esc}\xi_{ion} \approx 10^{24.2-24.6}$ Hz erg^{-1}. This is significantly higher than our upper limit of $f_{esc}\xi_{ion} \lesssim 10^{23.5}$ Hz erg^{-1} (using $\langle$f$_{esc}\rangle$ and ξ_{ion} where dust is corrected with M$_{star}$, see §5 and §6). However, as shown in §6.5, we expect $\xi_{ion} \approx 10^{25.4}$ Hz erg^{-1} in the reionization era due to the dependency of ξ_{ion} on EW(Hα), such that escape fractions of $f_{esc} \approx 10^{+6}_{-4}$ % would suffice for $f_{esc}\xi_{ion} \approx 10^{24.2}$ Hz erg^{-1}. Becker & Bolton (2013) find an evolution in the product of $f_{esc}\xi_{ion}$ of a factor 4 between $z = 3-5$ (similar to Haardt & Madau 2012), which is consistent with our measurements. This is because we find a factor of ≈ 1.5 evolution in ξ_{ion} over the redshift interval, and our measurements of $\langle$f$_{esc}\rangle$ are consistent with a factor ≈ 3 increase between $z = 2-5$.

Recently, Faisst (2016) inferred that f$_{esc}$ may evolve with redshift by combining a relation between f$_{esc}$ and the [OIII]/[OII] ratio with the inferred redshift evolution of the [OIII]/[OII] ratio. This redshift evolution is estimated from local analogs to high redshift galaxies selected on Hα EW, such that the redshift evolution of f$_{esc}$ is implicitly coupled to the evolution of Hα EW as in our model of $\xi_{ion}(z)$. Faisst (2016) estimate that f$_{esc}$ evolves from ≈ 2 % at $z = 2$ to ≈ 5 % at $z = 5$, which is consistent with our measurements of $\langle$f$_{esc}\rangle$ (see Fig. 5). With this evolving escape fraction, galaxies can provide sufficient amounts of photons to reionize the Universe, consistent with the most recent CMB constraints Planck Collaboration et al. (2016). This calculation assumes $\xi_{ion} = 10^{25.4}$ Hz erg^{-1}, which is the same value our model predicts for ξ_{ion} in the reionization era.

In addition to understanding whether galaxies have reionized the Universe, it is perhaps more interesting to understand which galaxies have been the most important to do so. For example, Sharma et al. (2016) argue that the distribution of escape fractions in galaxies is likely very bimodal and dependent on the SFR surface density, which could mean that LyC photons preferentially escape from bright galaxies. Such a scenario may agree better with a late and rapid reionization process such as favoured by the new low optical depth measurement from Planck Collaboration et al. (2016). As mentioned in §5.1, such a scenario where only a fraction of relatively rare galaxies (e.g. Sobral et al. 2015b) has a very high escape fraction and which thus provide the majority of the ionizing background agrees with our result that $\approx 5\%$ of the HAEs at $z = 2.2$ have f$_{esc} > 50$ %, which is enough to explain the globally average escape fraction, even if 95 % of star-forming galaxies have f$_{esc} = 0$.

To make progress we need a detailed understanding of the physical processes which drive f$_{esc}$, for which a significant sample of directly detected LyC leakers at a range of redshifts and galaxy properties is required. It is challenging to measure f$_{esc}$ directly at $z > 3$ (and practically impossible at $z > 5$) due to the increasing optical depth of the IGM with redshift, such that indirect methods to estimate f$_{esc}$ may be more successful (e.g. Jones et al. 2013; Zackrisson et al. 2013; Verhamme et al. 2015). However, the validity of these methods remains to be evaluated (c.f. Vasei et al. 2016).

8 CONCLUSIONS

We have studied the production and escape of ionizing photons (LyC, $\lambda_0 < 912$ Å) for a large sample of Hα selected galaxies at $z = 2.2$. Thanks to the joint coverage of the rest-frame LyC, UV and Hα (and, in some cases, Lyα and [OIII]), we have been able to reliably estimate the intrinsic LyC luminosity, constrain the escape fraction of ionizing photons (f$_{esc}$) and measure the number of ionizing photons per unit UV luminosity (ξ_{ion}) and study how these depend on galaxy properties. Our results are:

(i) We have identified 8 candidate LyC leakers among 191 HAEs with tentative f$_{esc} > 60$ %, after removing sources for which the *NUV* flux is possibly contaminated due to foreground sources with high-resolution *HST*/F814W imaging, such that ≈ 5 % of HAEs are candidate LyC leakers. Two LAEs are also candidate LyC leakers. High resolution UV imaging with *HST* is required to confirm our 10 candidates as real LyC leakers (§4.2).

(ii) We have stacked the *NUV* thumbnails for all HAEs and subsets of galaxies in order to obtain stronger constraints on f$_{esc}$. None of the stacks shows a direct detection of LyC flux, allowing us to place a median (mean) upper limit of f$_{esc} < 5.5 (12.7)$ % for the stack of star-forming HAEs (§5.3).

(iii) Combining the IGM emissivity measurements from Becker & Bolton (2013) with the integrated Hα luminosity function from Sobral et al. (2013) at $z = 2.2$, we find a globally averaged $\langle$f$_{esc}\rangle = 5.9^{+9.3}_{-2.6}$ % (§5). A global $\langle$f$_{esc}\rangle \approx 5$ % is consistent with 5 % of the HAEs having f$_{esc} \approx 75$ % (so ~ 95 % may have f$_{esc} \approx 0$).

(iv) Applying a similar analysis to published data at $z \approx 4-5$ results in a relatively constant f$_{esc}$ with redshift (see Table 3 and Fig. 5). We rule out $\langle$f$_{esc}\rangle > 20$ % at redshifts lower than $z \approx 5$. An additional contribution of ionizing photons from rare quasars strengthens this constraint.

(v) We find that ξ_{ion} increases strongly with increasing sSFR and Hα EW and decreasing UV luminosity, independently on the dust correction method. We find no significant correlations between ξ_{ion} and SFR(Hα), β or M$_{star}$. On average, LAEs have a higher ξ_{ion} than HAEs, a consequence of LAEs having typically bluer UV slopes, lower masses and lower values of E$(B-V)$ (§6) – properties which are typical for galaxies at the highest redshift.

(vi) The median ξ_{ion} of HAEs at $z = 2.2$ is $\xi_{ion} \approx 10^{24.77\pm0.04}$ Hz erg^{-1}, which is 0.4-0.5 dex lower than the typically assumed values in the reionization era or recent measurements at $z \sim 4-5$ (Bouwens et al. 2016), see Table 4. Only half of this difference is explained by the lower stellar mass and dust attenuation of the galaxies in the Bouwens et al. (2016) sample.

(vii) By combining our trend between ξ_{ion} and Hα EW with the redshift evolution of Hα EW, we find that ξ_{ion} increases with ≈ 0.2 dex between $z = 2.2$ and $z = 4-5$, resulting in perfect agreement with the results from Bouwens et al. (2016). Extrapolating this trend leads to a median value of $\xi_{ion} \approx 10^{25.4}$ Hz erg^{-1} at $z \sim 8$, slightly higher than the typically assumed value in the reionization epoch (§7), such that a relatively low global f$_{esc}$ (consistent with our global estimates at $z \approx 2-5$) would suffice to provide the photons to reionize the Universe.

ACKNOWLEDGMENTS

REFERENCES

Alexandroff R. M., Heckman T. M., Borthakur S., Overzier R., Leitherer C., 2015, ApJ, 810, 104
Astropy Collaboration et al., 2013, AAP, 558, A33
Atek H., et al., 2015, ApJ, 800, 18
Becker G. D., Bolton J. S., 2013, MNRAS, 436, 1023
Becker G. D., Bolton J. S., Madau P., Pettini M., Ryan-Weber E. V., Venemans B. P., 2015, MNRAS, 447, 3402
Bergvall N., Leitet E., Zackrisson E., Marquart T., 2013, AAP, 554, A38
Bertin E., 2010, SWarp: Resampling and Co-adding FITS Images Together, Astrophysics Source Code Library (ascl:1010.068)
Bertin E., Arnouts S., 1996, AAPS, 117, 393
Best P., et al., 2013, Astrophysics and Space Science Proceedings, 37, 235
Borthakur S., Heckman T. M., Leitherer C., Overzier R. A., 2014, Science, 346, 216
Boutsia K., et al., 2011, ApJ, 736, 41
Bouwens R. J., et al., 2011, ApJ, 737, 90
Bouwens R. J., et al., 2012, ApJL, 752, L5
Bouwens R. J., et al., 2015a, ApJ, 803, 34
Bouwens R. J., Illingworth G. D., Oesch P. A., Caruana J., Holwerda B., Smit R., Wilkins S., 2015b, ApJ, 811, 140
Bouwens R. J., Smit R., Labbe I., Franx M., Caruana J., Oesch P., Stefanon M., Rasappu N., 2016, preprint, (arXiv:1511.08504)
Bowler R. A. A., et al., 2014, MNRAS, 440, 2810
Bridge C. R., et al., 2010, ApJ, 720, 465
Bruzual G., Charlot S., 2003, MNRAS, 344, 1000
Buat V., et al., 2015, AAP, 577, A141
Calzetti D., Armus L., Bohlin R. C., Kinney A. L., Koornneef J., Storchi-Bergmann T., 2000, ApJ, 533, 682
Castellano M., et al., 2016, AAP, 590, A31
Cen R., Kimm T., 2015, ApJL, 801, L25
Chabrier G., 2003, PASP, 115, 763
Chen H.-W., Prochaska J. X., Gnedin N. Y., 2007, ApJL, 667, L125

Choudhury T. R., Puchwein E., Haehnelt M. G., Bolton J. S., 2015, MNRAS, 452, 261
Civano F., et al., 2012, ApJS, 201, 30
Conseil S., Vibert D., Amouts S., Milliard B., Zamojski M., Liebaria A., Guillaume M., 2011, in Evans I. N., Accomazzi A., Mink D. J., Rots A. H., eds, Astronomical Society of the Pacific Conference Series Vol. 442, Astronomical Data Analysis Software and Systems XX. p. 107
Cooke J., Ryan-Weber E. V., Garel T., Díaz C. G., 2014, MNRAS, 441, 837
Cowie L. L., Barger A. J., Trouille L., 2009, ApJ, 692, 1476
Cristiani S., Serrano L. M., Fontanot F., Koothrappali R. R., Vanzella E., Monaco P., 2016, preprint, (arXiv:1603.09351)
De Barros S., et al., 2016, AAP, 585, A51
Deharveng J.-M., Buat V., Le Brun V., Milliard B., Kunth D., Shull J. M., Gry C., 2001, AAP, 375, 805
Domínguez A., et al., 2013, ApJ, 763, 145
Duncan K., Conselice C. J., 2015, MNRAS, 451, 2030
Faisst A. L., 2016, preprint, (arXiv:1605.06507)
Faisst A. L., et al., 2016, preprint, (arXiv:1601.07173)
Fan X., et al., 2006, AJ, 132, 117
Ferrara A., Loeb A., 2013, MNRAS, 431, 2826
Finkelstein S. L., 2015, preprint, (arXiv:1511.05558)
Finkelstein S. L., et al., 2015, ApJ, 810, 71
Förster Schreiber N. M., et al., 2009, ApJ, 706, 1364
Fumagalli M., et al., 2012, ApJL, 757, L22
Garn T., Best P. N., 2010, MNRAS, 409, 421
Geach J. E., Smail I., Best P. N., Kurk J., Casali M., Ivison R. J., Coppin K., 2008, MNRAS, 388, 1473
Giallongo E., et al., 2015, AAP, 578, A83
Grazian A., et al., 2016, AAP, 585, A48
Guaita L., et al., 2016, AAP, 587, A133
Haardt F., Madau P., 2012, ApJ, 746, 125
Hunter J. D., 2007, Computing In Science & Engineering, 9, 90
Ibar E., et al., 2013, MNRAS, 434, 3218
Ilbert O., et al., 2009, ApJ, 690, 1236
Inoue A. K., Iwata I., Deharveng J.-M., 2006, MNRAS, 371, L1
Inoue A. K., Shimizu I., Iwata I., Tanaka M., 2014, MNRAS, 442, 1805
Ishigaki M., Kawamata R., Ouchi M., Oguri M., Shimasaku K., Ono Y., 2015, ApJ, 799, 12
Izotov Y. I., Schaerer D., Thuan T. X., Worseck G., Guseva N. G., Orlitova I., Verhamme A., 2016a, preprint, (arXiv:1605.05160)
Izotov Y. I., Orlitová I., Schaerer D., Thuan T. X., Verhamme A., Guseva N. G., Worseck G., 2016b, Nature, 529, 178
Jones E., Oliphant T., Peterson P., et al., 2001, SciPy: Open source scientific tools for Python, http://www.scipy.org/
Jones T. A., Ellis R. S., Schenker M. A., Stark D. P., 2013, ApJ, 779, 52
Kashino D., et al., 2013, ApJL, 777, L8
Kennicutt Jr. R. C., 1998, ARAA, 36, 189
Khaire V., Srianand R., Choudhury T. R., Gaikwad P., 2016, MNRAS, 457, 4051
Khostovan A. A., Sobral D., Mobasher B., Smail I., Darvish B., Nayyeri H., Hemmati S., Stott J. P., 2016, preprint, (arXiv:1604.02456)
Koekemoer A. M., et al., 2007, ApJS, 172, 196
Koyama Y., et al., 2015, MNRAS, 453, 879
Kuhlen M., Faucher-Giguère C.-A., 2012, MNRAS, 423, 862
Leitet E., Bergvall N., Hayes M., Linné S., Zackrisson E., 2013, AAP, 553, A106
Leitherer C., Ferguson H. C., Heckman T. M., Lowenthal J. D., 1995, ApJL, 454, L19
Leitherer C., et al., 1999, ApJS, 123, 3
Leitherer C., Ekström S., Meynet G., Schaerer D., Agienko K. B., Levesque E. M., 2014, ApJS, 212, 14

Leitherer C., Hernandez S., Lee J. C., Oey M. S., 2016, preprint, (arXiv:1603.06779)

Lilly S. J., et al., 2009, ApJS, 184, 218

Livermore R. C., Finkelstein S. L., Lotz J. M., 2016, preprint, (arXiv:1604.06799)

Ma X., Kasen D., Hopkins P. F., Faucher-Giguère C.-A., Quataert E., Kereš D., Murray N., 2015, MNRAS, 453, 960

Madau P., Dickinson M., 2014, ARAA, 52, 415

Madau P., Haardt F., 2015, ApJL, 813, L8

Madau P., Haardt F., Rees M. J., 1999, ApJ, 514, 648

Marmol-Queralto E., McLure R. J., Cullen F., Dunlop J. S., Fontana A., McLeod D. J., 2015, preprint, (arXiv:1511.01911)

Martin C., et al., 2003, in Blades J. C., Siegmund O. H. W., eds, PROCSPIE Vol. 4854, Future EUV/UV and Visible Space Astrophysics Missions and Instrumentation.. pp 336–350, doi:10.1117/12.460034

Martin D. C., et al., 2005, ApJL, 619, L1

Matthee J., Sobral D., Santos S., Röttgering H., Darvish B., Mobasher B., 2015, MNRAS, 451, 400

Matthee J., Sobral D., Oteo I., Best P., Smail I., Röttgering H., Paulino-Afonso A., 2016, MNRAS, 458, 449

McCracken H. J., et al., 2010, ApJ, 708, 202

McGreer I. D., Mesinger A., D'Odorico V., 2015, MNRAS, 447, 499

McLeod D. J., McLure R. J., Dunlop J. S., Robertson B. E., Ellis R. S., Targett T. A., 2015, MNRAS, 450, 3032

McLure R. J., et al., 2013, MNRAS, 432, 2696

Meurer G. R., Heckman T. M., Calzetti D., 1999, ApJ, 521, 64

Micheva G., Iwata I., Inoue A. K., 2016, preprint, (arXiv:1604.00102)

Mitra S., Ferrara A., Choudhury T. R., 2013, MNRAS, 428, L1

Mitra S., Choudhury T. R., Ferrara A., 2015, MNRAS, 454, L76

Mostardi R. E., Shapley A. E., Steidel C. C., Trainor R. F., Reddy N. A., Siana B., 2015, ApJ, 810, 107

Mowlavi N., Eggenberger P., Meynet G., Ekström S., Georgy C., Maeder A., Charbonnel C., Eyer L., 2012, AAP, 541, A41

Muzzin A., et al., 2013, ApJs, 206, 8

Nakajima K., et al., 2012, ApJ, 745, 12

Oteo I., Sobral D., Ivison R. J., Smail I., Best P. N., Cepa J., Pérez-García A. M., 2015, MNRAS, 452, 2018

Paardekooper J.-P., Khochfar S., Dalla Vecchia C., 2015, MN-RAS, 451, 2544

Pannella M., et al., 2015, ApJ, 807, 141

Pawlik A. H., Schaye J., Dalla Vecchia C., 2015, MNRAS, 451, 1586

Planck Collaboration et al., 2016, preprint, (arXiv:1605.03507)

Price L. C., Trac H., Cen R., 2016, preprint, (arXiv:1605.03970)

Puglisi A., et al., 2016, AAP, 586, A83

Reddy N. A., Steidel C. C., 2009, ApJ, 692, 778

Reddy N. A., et al., 2015, ApJ, 806, 259

Robertson B. E., et al., 2013, ApJ, 768, 71

Robertson B. E., Ellis R. S., Furlanetto S. R., Dunlop J. S., 2015, ApJL, 802, L19

Rutkowski M. J., et al., 2016, ApJ, 819, 81

Sandberg A., Östlin G., Melinder J., Bik A., Guaita L., 2015, ApJL, 814, L10

Sanders R. L., et al., 2015, ApJ, 799, 138

Schaerer D., 2002, AAP, 382, 28

Schaerer D., 2003, AAP, 397, 527

Scoville N., et al., 2007, ApJS, 172, 38

Sharma M., Theuns T., Frenk C., Bower R., Crain R., Schaller M., Schaye J., 2016, MNRAS,

Shivaei I., Reddy N. A., Steidel C. C., Shapley A. E., 2015, ApJ, 804, 149

Siana B., et al., 2007, ApJ, 668, 62

Siana B., et al., 2015, ApJ, 804, 17

Smit R., et al., 2014, ApJ, 784, 58

Smit R., Bouwens R. J., Labbé I., Franx M., Wilkins S. M., Oesch P. A., 2015, preprint, (arXiv:1511.08808)

Smith B. M., et al., 2016, preprint, (arXiv:1602.01555)

Sobral D., et al., 2009, MNRAS, 398, L68

Sobral D., Best P. N., Matsuda Y., Smail I., Geach J. E., Cirasuolo M., 2012, MNRAS, 420, 1926

Sobral D., Smail I., Best P. N., Geach J. E., Matsuda Y., Stott J. P., Cirasuolo M., Kurk J., 2013, MNRAS, 428, 1128

Sobral D., Best P. N., Smail I., Mobasher B., Stott J., Nisbet D., 2014, MNRAS, 437, 3516

Sobral D., et al., 2015a, MNRAS, 451, 2303

Sobral D., Matthee J., Darvish B., Schaerer D., Mobasher B., Röttgering H. J. A., Santos S., Hemmati S., 2015b, ApJ, 808, 139

Sobral D., et al., 2016a, in prep

Sobral D., Stroe A., Koyama Y., Darvish B., Calhau J., Afonso A., Kodama T., Nakata F., 2016b, MNRAS, 458, 3443

Stanway E. R., Eldridge J. J., Becker G. D., 2016, MNRAS, 456, 485

Steidel C. C., Pettini M., Adelberger K. L., 2001, ApJ, 546, 665

Steidel C. C., Bogosavljević M., Shapley A. E., Kollmeier J. A., Reddy N. A., Erb D. K., Pettini M., 2011, ApJ, 736, 160

Swinbank A. M., Sobral D., Smail I., Geach J. E., Best P. N., McCarthy I. G., Crain R. A., Theuns T., 2012, MNRAS, 426, 935

Taylor M., 2013, Starlink User Note, 253

Van Der Walt S., Colbert S. C., Varoquaux G., 2011, preprint, (arXiv:1102.1523)

Vanzella E., et al., 2012, ApJ, 751, 70

Vanzella E., et al., 2016, preprint, (arXiv:1602.00688)

Vasei K., et al., 2016, preprint, (arXiv:1603.02309)

Verhamme A., Orlitová I., Schaerer D., Hayes M., 2015, AAP, 578, A7

Weigel A. K., Schawinski K., Treister E., Urry C. M., Koss M., Trakhtenbrot B., 2015, MNRAS, 448, 3167

Wuyts S., et al., 2011, ApJ, 738, 106

Zackrisson E., Inoue A. K., Jensen H., 2013, ApJ, 777, 39

Zamojski M. A., et al., 2007, ApJS, 172, 468

APPENDIX A: THUMBNAIL IMAGES

In Fig. A1 we show thumbnail images of all our candidate LyC leakers from the sample of isolated HAEs. The thumbnail images of the stacks of all isolated star-forming HAEs are shown in Fig. A2.

APPENDIX B: REDSHIFT EVOLUTION OF ξ_{ION} WITH DIFFERENT DUST CORRECTIONS

In Fig. B1 we show the inferred redshift evolution of ξ_{ion} when we apply different methods to correct ξ_{ion} for dust. Most of the differences are caused by a varying normalisation of ξ_{ion}, since we find that the slope of the fit between ξ_{ion} and Hα EW varies only mildly for various dust correction methods, see Table 5. However, we note again that most independent observations from Balmer decrements and *Herschel* prefer dust attenuations similar to the dust attenuation we use when correcting for dust with stellar mass. We note that the β-method gives good agreement with the measured ξ_{ion} from Bouwens et al. (2016), who also applied this method.

This paper has been typeset from a TeX/LaTeX file prepared by the author.
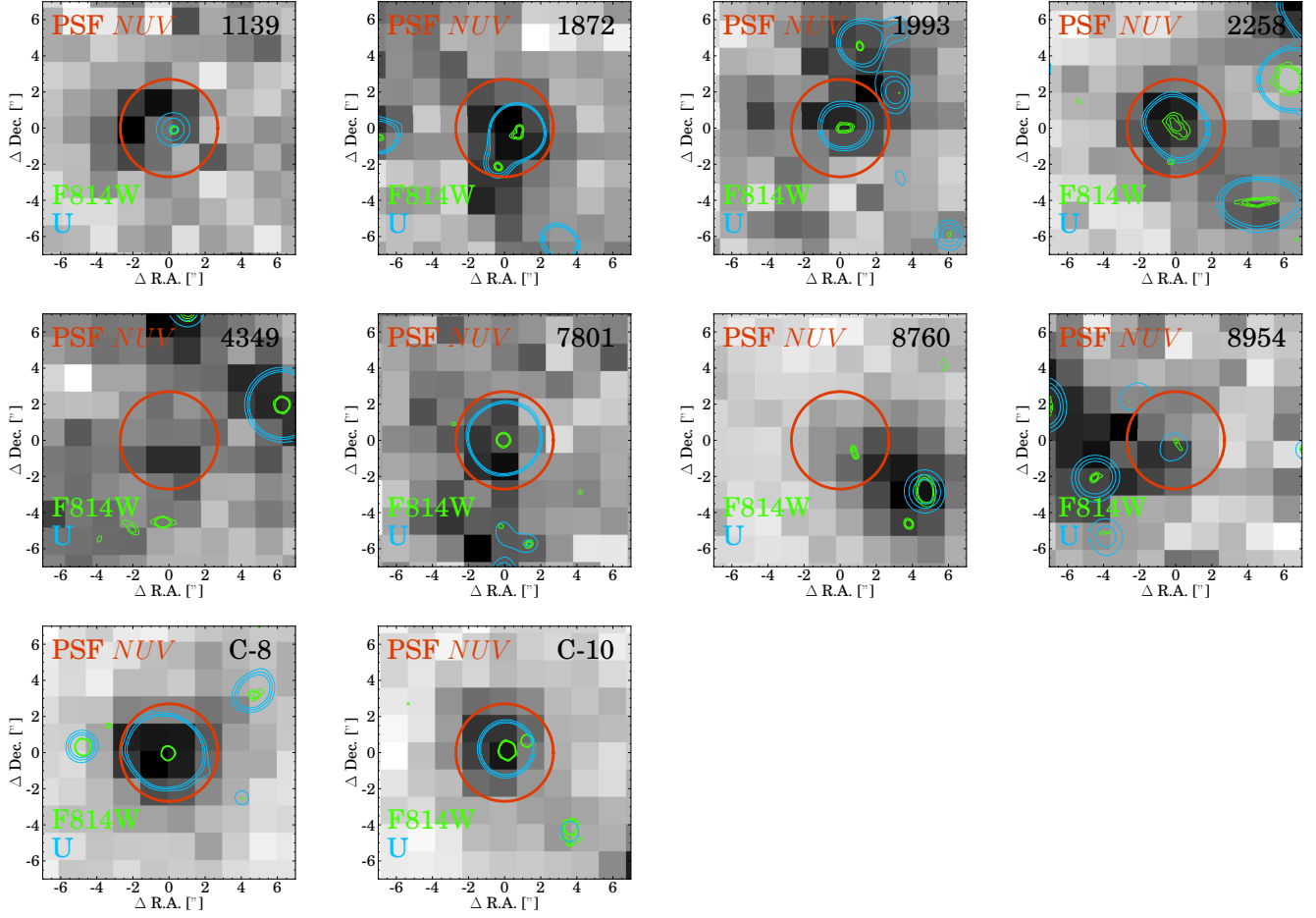
Figure A1. $15 \times 15''$ thumbnail images of all isolated LyC leaker candidates Hα and Lyα emitters at $z = 2.2$, centered on the positions of the HAE/LAE. The background image shows the counts in *GALEX NUV* imaging. The green contours correspond to the 3, 4 and 5 σ contours in the HST/ACS F814W image, smoothed with the PSF FWHM of $0.09''$ (Scoville et al. 2007), while the blue contours are from CFHT/U band imaging (McCracken et al. 2010). The red circle shows the PSF of the *NUV* image. The images are annotated with the IDs of the galaxies in the HiZELS catalogue (Sobral et al. 2013). Lyα emitters are identified with a "C". IDs 1139, 1993 and 7801 are detected in both Hα and Lyα. IDs 1139 and 7801 are X-ray AGN. ID 4349 has a neighbouring source with a photometric redshift of 2.2, although this is not selected as Hα emitter. None of the other LyC leaker candidates has neighbouring sources at the same redshift: all other sources seen in thumbnails have photometric redshifts of < 1.5.
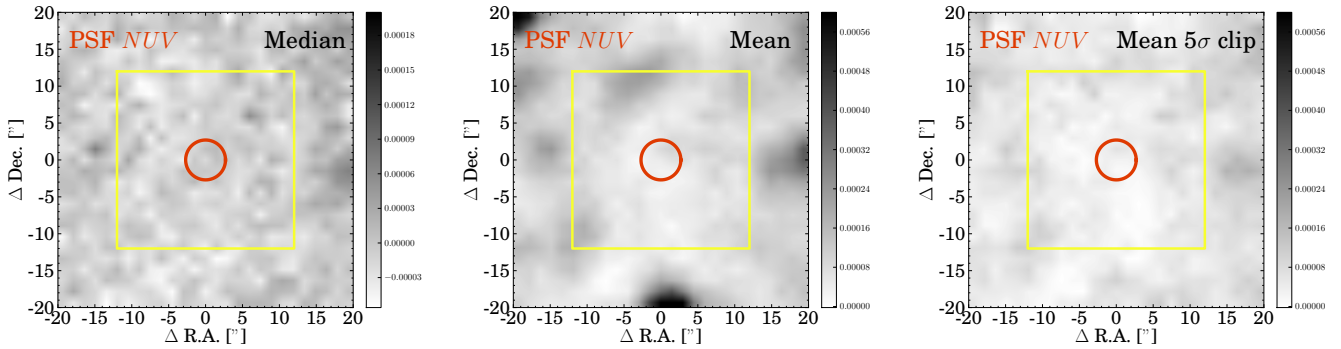

Figure A2. $20 \times 20''$ thumbnail images of the *NUV* stack for CLEAN, star-forming HAEs in COSMOS, for three different stacking methods. The red circle shows the PSF of *NUV* on the central position. The yellow box is the box which is used to measure the depth of the stack. Note that the color bar of the median stack is different than the color bar of the mean stack. Counts can be converted to AB magnitude with a ZP of 20.08.
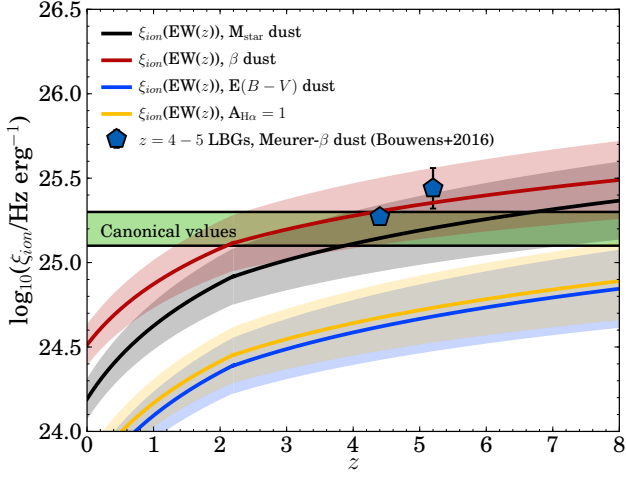
Figure B1. Inferred evolution of ξ_{ion} with redshift based on the EW(Hα) evolution from Faisst et al. (2016) and our observed trend between ξ_{ion} and Hα EW for HAEs with $M_{star} \sim 10^{9.2}$ $M_{\odot}$, for different methods to correct for dust. The black line shows the results when correcting for dust with M_{star}, the red line shows dust corrected with β, the blue line shows dust corrected with the $E(B-V)$ values from SED fitting and the yellow line shows the results when we apply a global correction of $A_{H\alpha} = 1$. The shaded regions indicate the errors on the redshift evolution of ξ_{ion}.